ACS OMEGA

http://pubs.acs.org/journal/acsodf

Review

Review of Thermoresponsive Electroactive and Magnetoactive Shape Memory Polymer Nanocomposites

Clara Pereira Sánchez,* Christine Jérôme,* Ludovic Noels,* and Philippe Vanderbemden*

Cite This: https://doi.org/10.1021/acsomega.2c05930

Read Online

ACCESS | Metrics & More | Article Recommendations

ABSTRACT: Electroactive and magnetoactive shape memory polymer nanocomposites (SMCs) are multistimuli-responsive smart materials that are of great interest in many research and industrial fields. In addition to thermoresponsive shape memory polymers, SMCs include nanofillers with suitable electric and/or magnetic properties that allow for alternative and remote methods of shape memory activation. This review discusses the state of the art on these electro- and magnetoactive SMCs and summarizes recently published investigations, together with relevant applications in several fields. Special attention is paid to the shape memory characteristics (shape fixity and shape recovery or recovery force) of these materials, as well as to the magnitude of the electric and magnetic fields required to trigger the shape memory characteristics.

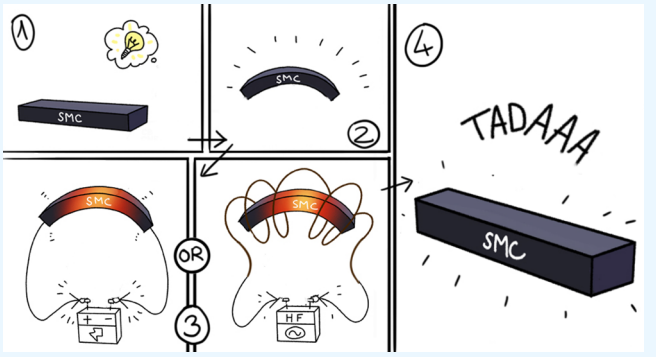

1. INTRODUCTION

Shape memory polymers (SMPs) and their composites (SMCs) are smart materials that are able to respond to certain external stimuli by changing their shape. In most cases, these shape memory materials (SMMs) are thermoresponsive, meaning that their shape memory properties are triggered depending on their temperature. Other response methods exist such as light, pH, and solvents,[1] but these will not be covered in this review. The simplest shape memory cycle of a thermoresponsive SMM is composed of a shape programming step and a shape recovery step. The shape programming step starts with the SMM in its original shape, commonly termed the permanent shape, that is heated above its transition temperature (T_{trans}). The T_{trans} values of a SMM are those related to the phase transitions that control the shape memory process: i.e., the glass transition or the melting−crystallization transition. Once at a temperature passes T_{trans}, a stress is applied, leading to a deformation from the permanent shape to the desired temporary shape. The shape programming step finishes by cooling the material under stress below T_{trans} while maintaining said deformation in order to fix the temporary shape, after which the applied stress can be released. Reheating the material above T_{trans} leads to the shape recovery from the temporary shape to the permanent shape due to stress relaxation.[2]

Conventionally, the shape recovery is triggered with direct heating by placing the SMM close to a heat source (e.g., inside an oven). This technique, which relies on an external heater, is occasionally impossible, problematic, or even dangerous. In recent years, much effort has been put into remotely inducing the shape recovery by indirectly heating the SMM using an electric or a magnetic field.[3] However, pristine SMPs are not suitable for these remote actuation triggers because of their high electric resistivity and insensitivity to magnetic fields, akin to the properties of conventional polymers. In order to benefit from these alternative heating mechanisms, either high electrical conductivity or magnetic fillers are embedded within the SMPs, hence conforming a SMC. For conciseness, SMM is used in the remainder of the article to refer to SMPs and SMCs.

In this review, we address the topic of shape memory polymer nanocomposites activated by an electric or magnetic field. We start with a brief introduction and overview on the topic of shape memory and the different types of shape memory behavior: one-way, two-way, and multiple shape memory. We continue by addressing the phenomena responsible for electro- and magnetoactivation of SMMs. After this theoretical introduction, we discuss the typical nanofillers used to disperse within the polymer matrix in order to confer electroactive and magnetoactive properties to SMCs. Some of the numerous works published in the past few years are summarized, paying special attention to the shape memory characteristics and the

Received: September 13, 2022
Accepted: October 13, 2022

magnitude of the electric or magnetic fields required for activation. As an additional tool for the reader, an extensive table of additional references on these SMMs is available in the Appendix. Some recent progress and applications of these SMCs are discussed next. Finally, future horizons and challenges in the investigation of SMMs are pointed out.

2. BASIC CONCEPTS ON SMPS AND THEIR COMPOSITES

The shape memory effect is a result of an adequate polymer molecular architecture including two parts: (i) the netpoints that build up the permanent shape of the SMP and (ii) the molecular-switchable segments that are responsible for fixing the temporary shape of the SMP.[4] The netpoints are cross-links that can be either chemical (covalent bonds) or physical. The latter is related to interactions among the molecules of the polymer network that consists of crystallites, hydrogen bonds, or ionic interactions. Physically cross-linked netpoints are weaker than their covalent chemical counterpart; thus, thermoplastics are more prone to incomplete shape recovery.[5] Regarding the switchable segments, they are reversible cross-links that can also be of physical or chemical nature.

Depending on the nature of both the netpoints and the switchable segments, a comprehensive SMP classification consisting of four classes was introduced by the research group of Mather[6] and since reported by many others.[1,4,7−10] The classes are (I) glassy covalently cross-linked thermosets, (II) semicrystalline covalently cross-linked polymer networks, (III) glassy physically cross-linked copolymers and blends, and (IV) semicrystalline physically cross-linked block copolymers.

The T_{trans} of a SMM is the characteristic temperature related to the formation and destruction of the switchable segments. In general, the T_{trans} of semicrystalline SMPs is related to the melting−crystallization phase transition, i.e. the melting temperature (T_m) during heating and the crystallization temperature (T_c) during cooling. On the other hand, the T_{trans} of glassy SMPs is related to the glass transition temperature (T_g). These glassy SMPs usually have a broader T_{trans} range than semicrystalline-network SMPs and therefore a slower recovery. Although this may be regarded as an undesirable feature, in combination with the biocompatibility of some of these polymer networks, it makes them excellent candidates for biomedical applications.[11−13] Nevertheless, they are not ideal for applications where a fast shape recovery is needed. On the other hand, traditionally, the majority of covalent bonds are strong chemical cross-links that are stable and hard to break. Thus, most polymers that are covalently cross-linked cannot be recycled or reprocessed. In order to overcome the disadvantages associated with covalent cross-links while still having a strong bond among molecules, dynamic covalent bonds can be incorporated in SMPs. Dynamic covalent bonds are reversible and thus are able to be broken and formed when they are subjected to certain stimuli such as heat, light, or pH. In recent years more and more polymers have been produced incorporating dynamic covalent bonds in order to achieve materials that can self-heal, reshape for 3D printing purposes, and have shape memory.[14] There is a wide choice of methods to obtain dynamic covalent bonds, and the corresponding literature[14−18] is available.

2.1. The Basic Shape Memory Effect. The shape memory effect of a SMM arises after the shape programming process that is achieved in three steps. To aid in the explanation, the stress evolution with applied strain of a SMP is illustrated in Figure 1.

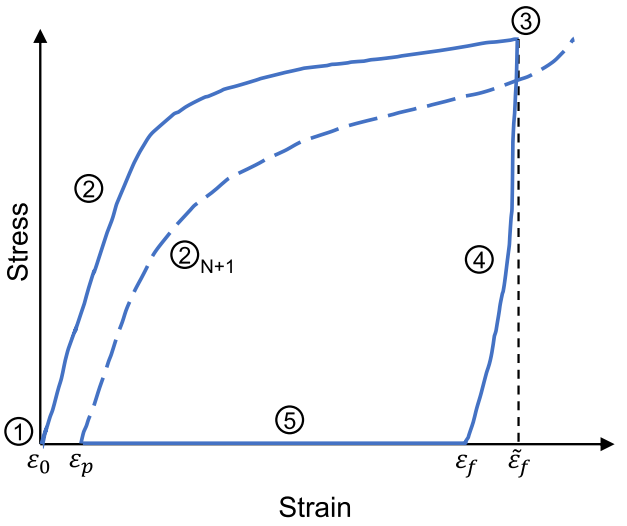

Figure 1. Illustration of the stress vs strain curve of a SMM during two conventional consecutive shape memory cycles performed under uniaxial tension. The marked strain levels ε_0, ε_p, ε_f, and $\tilde{\varepsilon}_f$ are used to calculate the shape fixity and shape recovery ratios.

The shape programming process starts by ① heating the material, initially in its permanent shape, above a characteristic T_{trans} (either T_g or T_m depending on the polymer). Second, ② a mechanical deformation is applied on the material while it is above T_{trans}. This mechanical deformation leads to a strain denoted by $\tilde{\varepsilon}_f$ in Figure 1. Finally, the programming process finishes by ③ cooling the material below T_{trans} while maintaining the desired load or the desired deformation. ④ Unloading the sample toward zero stress may result in a fixed strain ε_f slightly lower than $\tilde{\varepsilon}_f$. After this programming process is finished, the shape memory material is fixed in its new deformed temporary shape. During the applied deformation, the SMP, with either an amorphous or semicrystalline structure, is in the rubbery state and has a rubber-like behavior. In other words, the SMP above its T_{trans} exhibits entropic elasticity. Entropic elasticity exists while deforming an elastomer (or a SMP in the amorphous state) because the high mobility of the polymer chains permits the originally disordered structure to align in the direction of deformation.[19] Ordering the polymeric chains decreases the entropy of the material, and this energetic state gets fixed by vitrification or crystallization upon cooling the material below T_{trans}.

During the shape memory programming step, the shape memory material has stored energy due to the freezing of the lower entropic polymer network. The new temporary deformed shape can be viewed as a metastable shape: when the material is exposed to a certain external stimulus, the stored energy will be released. ⑤ Reheating the SMM above T_{trans} will cause a shape change back toward the permanent shape. This process, in which the material recovers the preferred high entropic state, is called shape recovery. Different temporary shapes can be attained by repeating the programming process with a different deformation step. Nevertheless, the primary permanent shape is always approximately recovered during the shape memory cycle. This is because T_{trans} only affects the switchable links that are related to the temporary shape, whereas the permanent shape is dictated by the netpoints of the SMM. Any damage on the netpoints during the shape memory cycle, for instance breaking of the netpoints due to excessive deformation in the shape

https://doi.org/10.1021/acsomega.2c05930
ACS Omega XXXX, XXX, XXX−XXX

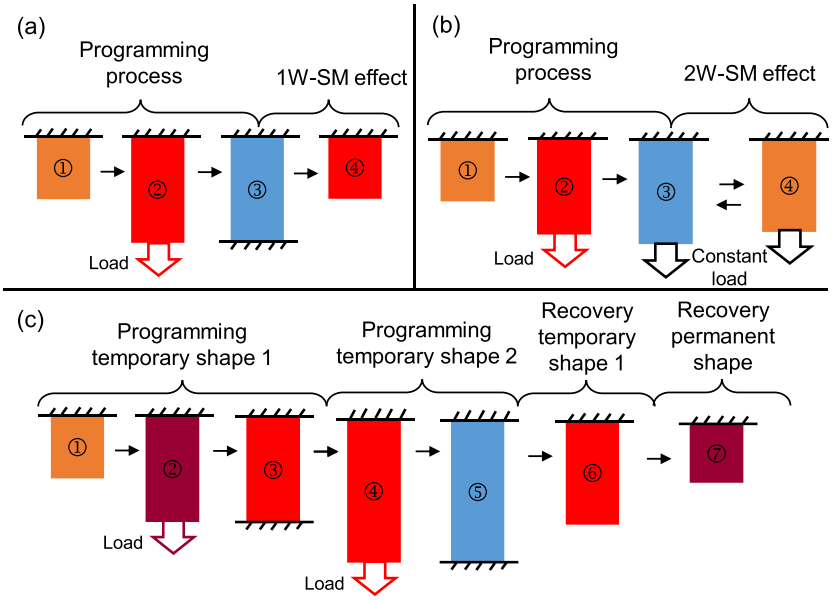

Figure 2. Illustration of the most common shape memory behaviors of SMMs: (a) one-way shape memory effect; (b) two-way shape memory effect; (c) multiple shape memory effect.

programming process, may cause the recovered permanent shape to slightly differ from the original permanent shape.

Two quantities are commonly used to evaluate the quality of a SMM: the shape fixity (R_F) and shape recovery ratios (R_R). They are calculated using eqs 1 and 2, respectively.

$$R_F = \frac{\varepsilon_f}{\tilde{\varepsilon}_f} \quad (1)$$

$$R_R = \frac{\tilde{\varepsilon}_f - \varepsilon_p}{\tilde{\varepsilon}_f - \varepsilon_0} \quad (2)$$

The shape fixity ratio quantifies the ability of the SMM to fix the temporary shape and it is calculated as the ratio of strain at the end of ③ cooling (ε_f indicated in Figure 1) over the strain at the end of ② elongation ($\tilde{\varepsilon}_f$ in Figure 1). On the other hand, the shape recovery ratio gives an idea of how well the SMM "remembers" its permanent shape by relating the strain during shape recovery to the strain due to elongation.

2.2. Types of Shape Memory Behavior. The shape memories presented in this section include the simplest one-way shape memory (1W-SM) effect. This section will also define the more complex shape memory behaviors commonly found in the literature, namely the two-way shape memory (2W-SM) effect and the multiple shape memory effect. An illustration of these behaviors is shown in Figure 2, and an explanation is provided next.

2.2.1. One-Way Shape Memory (1W-SM) Effect. The simple 1W-SM effect has already been explained in the previous sections. As illustrated in Figure 2a, it consists of a shape programming process composed by ① heating, ② deformation above T_{trans}, and ③ fixing of the temporary shape by cooling below T_{trans}. The programming process is followed by ④ reheating above T_{trans} with no load to trigger shape recovery toward the permanent shape. Once the shape recovery has been completed, the SMP is no longer thermoresponsive. To benefit from the shape memory effect again, another shape programming process needs to be performed on the material. Most shape memory polymers and their composites show this type of memory effect. In fact, it was believed until the late 2000s that only shape memory alloys but neither polymers nor their composites could show a two-way shape memory effect. Many examples of SMPs exhibiting the 1W-SM effect can be found in the literature.[20−25] Furthermore, a more exhaustive review on 1W-SM polymers and their composites has been given by Leng et al.[26]

2.2.2. Two-Way Shape Memory (2W-SM) Effect. The two-way shape memory (2W-SM) effect is present in some semicrystalline SMPs and their composites.[27,28] A typical 2W-SM effect under tension is illustrated in Figure 2b. The programming process is the same as for the 1W-SM effect: ① heating above T_{trans}, ② deformation above T_{trans}, and ③ cooling below T_{trans}. The 2W-SM effect in semicrystalline polymers arises, in general, by the cyclic ④ heating and ③ cooling above and below the respective T_{trans} at a constant load. In this case, the SMP is not left free to deform to the permanent shape but, instead, the shape keeps varying between a primary and a secondary temporary shape. The primary temporary shape is that obtained at the end of ② loading and recovered every time that the SMP is ④ reheated above its T_{trans} at constant load. The secondary temporary shape is that obtained by ③ cooling below T_{trans} at a constant load. The change in shape between the primary and the secondary temporary shapes can be repeated several times without the need of any other additional programming process.[13] The 2W-SM effect in semicrystalline polymers under constant tensile stress is characterized by a contraction of the material in the loading direction during heating above T_{trans}. Conversely, elongation along the loading direction is observed upon cooling below T_{trans}. Thus, the second temporary shape is longer than the first. Generally, if the reheating above T_{trans} happens in a stress-free configuration, the permanent shape is recovered, following the conventional 1W-SM effect.

In 2008, Chung, Romo-Uribe, and Mather[29] first reported the 2W-SM effect of a semicrystalline network of poly(cyclooctene) under constant stress. They showed that a lower cross-linking density would lead to a higher cooling-induced crystallization and, hence, a wider 2W-SM effect. Furthermore, T_m and T_c are

https://doi.org/10.1021/acsomega.2c05930
ACS Omega XXXX, XXX, XXX−XXX

found to be shifted to higher values on lowering the crystallization degree.

There is still disagreement on the mechanism behind the 2W-SM effect in semicrystalline polymer networks.[30] Most authors seem to agree on a melting-induced contraction and a crystallization-induced elongation as the (main) mechanism: oriented crystallites are formed in the direction of loading during cooling.[30,31] Chung, Romo-Uribe, and Mather postulated that the mechanism was a combination between crystallization-induced elongation and rubber elasticity.[29]

Generally, the 2W-SM effect is shown when the polymer is placed under nonzero stress.[28,30,32−42] Nevertheless, a few freestanding 2W-SM polymers have also been reported. These reports ascribe the freestanding 2W-SM effect to different sources, including two melting transitions, one broad melting transition, and chemically heterogeneous structures by creating thermostable crystallites after deformation-induced crystallization.[43−48] Furthermore, other types of materials such as liquid-crystalline elastomers[49,50] and shape memory composite laminates[51,52] have been described to exhibit 2W-SM effect.

2.2.3. Multiple Shape Effect. Triple shape memory materials are those that can utilize twice the 1W-SM effect in order to switch from a one temporary shape to another and from the latter to the permanent shape. A conventional 1W-SM effect is based on one T_{trans} for shape recovery. In the case of triple SMMs, the two shape changes are related to either one broad temperature interval for the transition or to two separated T_{trans} values. This is because a broad thermal transition can be regarded as an infinite amount of abrupt thermal transitions.[53,54]

For a triple SMM, two independent shape programming processes need to be followed. Figure 2c illustrates the typical procedure followed for a triple SMM based on the two transition temperatures $T_{trans,1}$ and $T_{trans,2}$ such that $T_0 > T_{trans,1} > T_{trans,2}$, where T_0 is the starting temperature. The deformation to obtain the two different temporary shapes in the illustration is applied by uniaxial tension. The first programming process consists of ① heating the SMM in its permanent shape at T_0 to a temperature above $T_{trans,1}$, where the polymer chains gain mobility, and ② the deformation to the first temporary shape can be applied. The deformation produces an orientation of the polymer chains along the loading direction, which in turn reduces the entropy of the material. This first temporary shape can be fixed by ③ cooling to a temperature T such that $T_{trans,1} > T > T_{trans,2}$, where the elastic energy is stored inside of the material thanks to the phase characterized by $T_{trans,1}$. The second programming process can start by ④ deforming the material once again while the temperature is between both T_{trans} values, which further decreases the entropy of the material. The second temporary shape is then fixed by ⑤ cooling below $T_{trans,2}$. Once again, the newly generated phase fixes the shape of the material and stores the extra elastic energy generated during step ④. If the freestanding material is ⑥ reheated above $T_{trans,2}$, its shape will change from the second to the first temporary shape due to the release of the energy stored during step ⑤. ⑦ A further increase in the temperature above $T_{trans,1}$ will reactivate the mobility of all polymer chains in the network, and the remaining stored energy will be released. This causes the shape recovery from the first temporary shape to the permanent shape.

In the last few years, several polymers have been reported to exhibit triple shape memory. Some examples of these materials based on a broad temperature interval can be found in the literature.[55−57] On the other hand, references on triple shape memory materials based on two individual T_{trans} values are also available.[58−60] Furthermore, the triple shape effect has also been observed in polymer laminates where each layer had a different T_{trans}.[61] A triple shape memory composite was created by Tobushi et al.[62] that functions as a bending actuator. It is a laminate of a mix of SMP and shape memory alloy (SMA) that bends in two different directions depending on which T_{trans}, that of the SMP or that of the SMA, was surpassed. As was already mentioned, conventional triple (or multiple) SMPs and SMCs are based on the 1W-SM effect,[63] thus making the shape memory effect an irreversible feature requiring the application of the programming processes for further shape change. Nevertheless, a novel triple SMP exhibiting 2W-SM is reported.[64]

The same concept can be extended to multiple (quadruple, quintuple, ...) SMMs by chaining more than two programming processes, hence leading to more shape recoveries. In general, this is done in polymer networks that present very broad transition temperature intervals.[56,65,66]

A few references are available reporting the cyclic quality of SMMs during a high number (≥1000) of 1W-SM[67] and 2W-SM[68] cycles, still showing remarkable shape memory characteristics. However, we have not found reports regarding a high number of cycle repetitions involving multiple shapes. Some reports address the R_F and R_R of multiple shape memory materials for the first ≤6 cycles.[55,58,59,64,69] Generally, it is observed that the R_F decreases and the R_R increases with each performed (sub)cycle. In comparing a triple SMM to a quadruple SMM, Dolog and Weiss reported a decrease of R_R and an increase of R_F when adding an extra shape to their cycle.[55] More research is needed on the repetition of cycles and subcycles of multiple shape memory materials in order to assess the lifetime and quality of the behavior of these materials upon extended use.

2.3. Electro- and Magnetoactivation. Up to now, the notions and definitions given in this section are common to thermally triggered SMMs, regardless of the type of activation. In electroactivated thermally triggered SMMs, the temperature is a result of Joule resistive heating, which requires the flow of an electric current I through a material with a certain electrical resistance R. The power dissipated P is the product $P = RI^2 = V^2/R$, where V is the voltage drop across the material. From the formula of the dissipated power, it is straightforward that, at finite voltages and currents, $P = 0$ either for a perfectly conducting ($R = 0$) or perfectly insulating ($R = \infty$) material. For resistive heating to take place, the material should ideally have a "medium" electrical resistance R, taking into account that reasonable values of currents (e.g., <100 mA) and voltages (e.g., <10 V) need to be used. In practice, reaching a dissipated power leading to a measurable temperature increase, e.g. $P \approx 0.1$ W, requires resistance values usually in the rage of ∼100−10000 Ω, which is significantly lower than the resistance of the polymer. Such resistance values are achieved by incorporating electrically conductive fillers in the insulating SMP matrix.

Another alternative way of triggering the heating of the material and, thus, the activation and shape recovery of SMCs is by the application of alternating magnetic fields. In order to obtain magnetosensitive SMCs, ferromagnetic fillers need to be incorporated inside the SMP. There are three magnetic heating mechanisms that can arise in magnetosensitive SMCs: (i) eddy currents, (ii) hysteresis, and (iii) losses related to the rotation of the magnetic spin due to Néel−Brown relaxation.[70] The heating efficiency is highly dependent on the size of the magnetic fillers. The composites with embedded fillers in the microscale can be heated through eddy current and hysteresis loss by applying

https://doi.org/10.1021/acsomega.2c05930
ACS Omega XXXX, XXX, XXX−XXX

magnetic fields at moderate frequencies. In contrast, when magnetic fillers in the nanoscale are introduced in the SMP, these two heating mechanisms become less effective. Hysteresis loss decreases and becomes negligible for particle diameters below a certain threshold. For instance, iron oxide (Fe_3O_4) turns superparamagnetic, i.e. the magnetization curve shows no hysteresis, for diameters smaller than 20 nm. Furthermore, a multidomain structure is theoretically estimated to happen for diameters higher than 62.9−128 nm.[71,72] These characteristic sizes depend on the nature and shape of the magnetic nanoparticles.

The main magnetic heating mechanism for magnetic nanoparticles is related to Néel−Brown relaxations. High frequencies are needed for this type of magnetic heating to generate a considerable temperature increase. The Néel relaxation consists of the rotation of the nanoparticle magnetic moment to align with the direction of the applied magnetic field while the nanoparticle itself stays motionless. The Brown relaxation leads to the physical rotation of the magnetic nanoparticles. Both relaxation mechanisms exist simultaneously when the particles are subjected to AC magnetic fields. Nevertheless, the Néel relaxation tends to dominate for smaller nanoparticles (<10 nm in diameter) in viscous media and Brownian motion tends to dominate for larger particles in media with low viscosities.[70,73]

3. ELECTRO- AND MAGNETOACTIVE SMCS: FILLERS AND ACTIVATION

SMPs are preferred over SMAs for various applications due to their low cost and their ability to sustain large deformations. Nevertheless, they also present some drawbacks or limitations in comparison to SMAs: SMPs have lower strength, stiffness, and recovery force and are electrically and thermally insulating. In order to overcome these limitations, different fillers have been incorporated within SMPs: hence, the terminology shape memory polymer composite. The addition of some of these fillers has been proven to improve some properties and give extra characteristics to the pristine polymers themselves. This includes the possibility of different types of stimuli for triggering the necessary temperature difference in order to make use of the shape memory properties. The properties of the resulting SMCs can be affected by several factors such as filler distribution, filler−polymer interface, filler size and aspect ratio, the nature of the SMP, and even the processing techniques.[74]

Regarding the size of the fillers, continuous fibers such as carbon, glass, or aramid fibers have been used to reinforce SMPs.[75−77] An alternative to continuous fibers is to use short (chopped) fibers[78,79] of a few millimeters in length. SMA wires or fibers have also been reported in the literature.[80] The fibers are generally incorporated within the SMP with the aim of improving the mechanical properties of the material. Even though not common, a few references have been found where carbon fibers, thanks to their high electrical conductivity, were also used to heat the SMC by means of electric Joule heating.[81−83] This review focuses on shape memory composites with dispersed nanofillers that are used in order to give the resulting nanocomposite the ability to be heated with an electric current or a magnetic field. A schematic diagram showing an overview of the main existing nanofillers is shown in Figure 3.

3.1. Carbon Nanofillers. In the past couple of decades, shape memory polymer nanocomposites with embedded carbon nanofillers have been intensely investigated to electrically induce the shape memory effect. Thanks to their excellent electrical

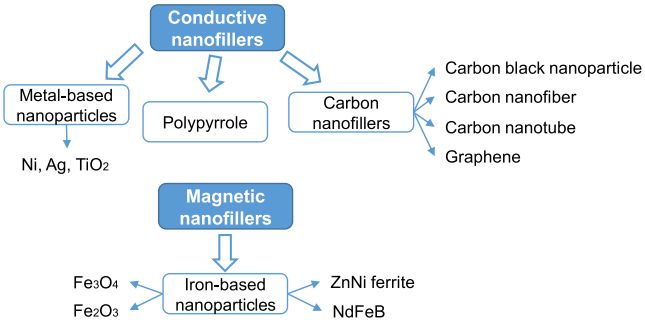

Figure 3. Main existing conductive and magnetic nanofillers reported in the literature to conform electro- and magnetoactive shape memory polymer composites.

conductivity, these nanofillers facilitate resistive heating and permit the electrical activation of the shape memory characteristics of SMCs. Moreover, the thermal conductivity of the resulting composite is improved. This feature is particularly interesting for applications where direct heat cannot be applied in order to trigger the shape memory effects. Such applications include, for instance, biomedical devices or self-deployable structures.[84] Within the group of carbon nanofillers, investigations focus on SMCs with embedded carbon black nanoparticles (CBs), carbon nanofibers (CNFs), single-walled and multiwalled carbon nanotubes (SWCNTs and MWCNTs, respectively), and graphene.

3.1.1. Carbon Black Nanoparticles. CBs are effective fillers that can be used for the reinforcement of shape memory polymers. Due to their spherical geometry, a high concentration of CBs is needed in order to surpass the percolation threshold. At low concentrations, the addition of CBs does not create an electrically conductive network that has the ability to heat due to an electric current. Nevertheless, concentrations of 0.5−1.0 vol % CBs have been shown to improve the actuation ratio of the 2W-SM effect and the elastic modulus at high temperature of a polyethylene-based SMC.[39] The same work showed that the 2W-SM effect of the composite was lost when the concentration of CB was increased to 20 vol %. At the required high concentrations for resistive heating at moderate voltages (>15 wt %), this family of SMCs was reported to have lower recovery ratios,[85] more brittle behavior leading to failure of the material at shorter deformations,[86,87] and, in some cases, severely worsened shape fixity.[88] The last effect is found in semicrystalline SMP composites, since the addition of CBs decreases the amount of crystalline regions within the composite,[39] which are in charge of fixing the temporary shape.

In order to achieve an electrical conducting network without a severe worsening of the shape memory characteristics of SMCs, other conductive fillers may be considered. Carbon nanotubes (CNTs) are an excellent alternative.

3.1.2. Carbon Nanotubes. CNTs are conductive fillers with other advantageous characteristics that enable the formation of SMCs with low electrical resistivity at low filler concentrations. This is due to the high aspect ratio of CNTs, which facilitates the formation of an electrically conductive network within the composite. In other words, the percolation threshold for nanocomposites using CNTs is attained at lower concentrations than for other conductive fillers such as CBs.[89] The resistivity once past this threshold for a given concentration of CNTs is also found to be lower than for other fillers at the same concentration. This can be advantageous, because a higher

https://doi.org/10.1021/acsomega.2c05930
ACS Omega XXXX, XXX, XXX−XXX

concentration of fillers may result in more brittle materials, high cost, high weight, or difficulty in processing due to an enormous increase in viscosity.

It also has been shown that, at the same concentrations, CNT-filled SMCs exhibit higher shape fixity than other fillers, such as CBs,[87] which may be attributed to the alignment of the CNTs in the direction of the deformation. In the same work, the authors also showed that their shape memory elastomer filled with CNTs displays a better shape recovery ratio and better overall shape memory characteristics, as can be seen in Figure 4. The

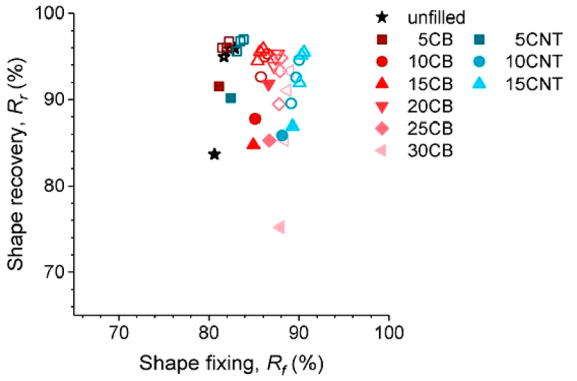

Figure 4. Relationship between the shape recovery ratio and the shape fixity ratio of a SMC with different concentrations (in phr) of CBs or CNTs (reproduced with permission from ref 87; published by MDPI, 2022.)

shape recovery was electrically triggered in their SMC with 15 parts per hundred rubber (phr) of CNTs at 50 V within 15 min. Conversely, the nature of the polymer matrix itself also influences the shape memory characteristics of the resulting composite. In a recent work, Tekay studied polymer blend networks of polycaprolactone (PCL) and a maleic anhydride grafted block copolymer (denominated SEBS-*g*-MA) with and without dispersed MWCNTs.[90] The author showed that varying the composition of the polymer network toward a 50/50 blend increases the recovery and fixity ratios. Changing the relative concentration to 30/70 of PCL/SEBS-*g*-MA decreased these ratios by 35% and 3%, respectively. The SMC with 10 phr MWCNTs has a resistivity of 0.0382 Ω m that is able to undergo electrically triggered shape recovery (91.17%) when it is subjected to a constant voltage of 40 V in 56 s.

The method of dispersion of the CNTs also plays an important role in the electrical and mechanical properties of the SMCs: investigations have focused on how to avoid CNT aggregation due to van der Waals forces and achieve a random but uniform dispersion within the composite. It has been shown that mini twin-screw melt mixing,[91] cross-linking MWCNTs onto semicrystalline networks,[92] *in situ* polymerization,[93] or surface modification[94] can decrease the electrical resistivity of the SMC. The last three methods also enhance the interfacial cohesiveness between the nanotubes and the polymer matrix, which is directly related to a better stress distribution and strength of the resulting composite. Nevertheless, surface modification should be used with caution since it may detrimentally affect the shape recovery ratio during the lifetime of the composite.[94] Furthermore, a decrease in the electrical resistivity with an aggressive functionalization of CNTs is due to the generation of defects on the surface of the nanotubes.

Another solution for creating a conductive network with carbon nanotubes is by incorporating them in films or yarns onto the polymer. These are commonly referred to as MWCNT nanopapers or buckypapers, which have been shown, for example in the work of Lu and Gou,[95] to facilitate the electrical activation of the shape memory composite when it is subjected to a constant current of 0.6 A or by Lu et al.[96] to trigger the shape recovery of a composite at a constant voltage of 30 V while driving up a weight of 5 g by 30 mm. In another investigation, a shape memory epoxy matrix with MWCNT nanopaper was quickly cured by heating with an electric field at constant voltage, reaching 105 °C at 4.5 V.[97] The electrical properties of the resulting composite were used once again to electrically trigger the shape recovery. A high concentration of 30 wt % MWCNTs could be embedded in the form of buckypaper in an epoxy shape memory polymer.[98] This SMC has an elastic modulus 52% and 514% higher than the pristine material below and above the T_{trans}, respectively. It shows shape recovery when it is subjected to 12 V under 22 s.

Wang et al. reported on a novel way of fabricating CNT-filled polyurethane SMC by spraying-evaporation modeling.[99] They printed CNT layers at different desired locations of the SMC. Several CNT layers can be printed in order to tailor the electrical resistivity of certain regions. More layers signify a lower electrical resistivity and higher temperature due to resistive heating whenever the material is subjected to a constant electrical current. They show a temperature difference of 12 °C along a single stripe of SMC between the regions with 10 and 50 CNT layers, as shown in Figure 5. This way, sequential and selectively triggered SMCs can be produced. They report complete shape recovery under 30 s when the SMCs are subjected to 40 V.

In the resistive heating phenomenon, the heat generated within the material directly depends on the injected electrical current and the electrical resistivity of the material. A thorough investigation on the phenomenon of resistive heating of an electroactive SMC was recently carried out by our group, including surface temperature measurements on a polycaprolactone SMP with 3 wt % MWCNTs used to validate analytical formulas and a 3D thermoelectric numerical model.[100] This investigation shows that the electrical resistivity of the SMC has a nonlinear nonmonotonic dependency on temperature. Other

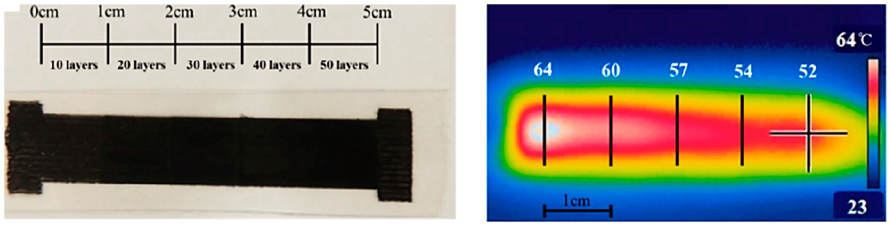

Figure 5. Stripe of a shape memory nanocomposite of polyurethane with different numbers of printed carbon nanotube layers along its length and the resulting temperature distribution due to resistive heating (reprinted from ref 99 with permission of Elsevier.)

https://doi.org/10.1021/acsomega.2c05930
ACS Omega XXXX, XXX, XXX−XXX

material properties such as the heat capacity or the thermal conductivity are also shown to affect the resulting temperature of the SMC. We also used a bespoke tensile test bench with integrated controllers for resistive heating in order to investigate the evolution of the electrical resistivity of the same SMC during 1W-SM cycles performed with uniaxial tensile deformation.[101] Using a proposed dedicated PI controller, the resulting temperature on the surface of the SMC due to resistive heating can be efficiently and accurately controlled in order to follow a certain heating/cooling ramp or in order to maintain a constant temperature even though the electrical resistivity varies with time. The results presented in ref 101 give also indications of the interplay among the electrical, thermal, and mechanical properties of the electroactive composite within shape memory cycles. An example of this interplay is shown in Figure 6, where

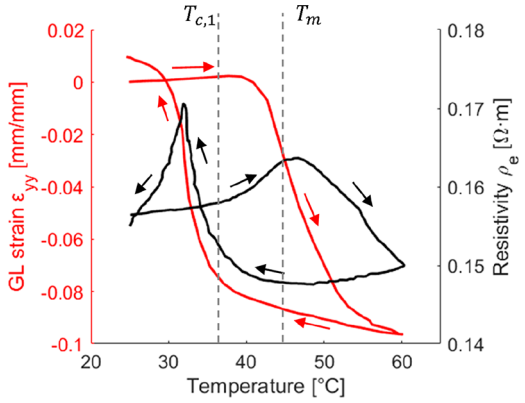

Figure 6. Evolution of the Green−Lagrange strain in the loading direction (ε_{yy} in red) and of the instantaneous electrical resistivity (ρ_e in black) with temperature of an SMP of polycaprolactone with 3 wt % MWCNTs. The test was performed at a constant stress of 600 kPa in order to study the 2W-SM cycle.

the strain in the loading direction is shown as a function of a thermal cycle performed at a constant stress of 600 kPa in order to investigate the 2W-SM characteristics of the SMC. The electrical resistivity during the process is also depicted. Further information on these measurements can be found in ref 101.

The energetic efficiency of the resistive heating process has been studied by Cortés et al.[102] for a thermosetting epoxy SMP with 0.2 wt % MWCNTs. Furthermore, because the heating can be generated locally in the surfaces of interest, this last work also illustrates the ability of sequentially activating the shape recovery of different regions within a SMC plate, as shown in Figure 7, under a voltage in the range 126−265 V. The same research group studied the IR-activated shape recovery of printed shape memory acrylic resins with 0.1 wt % MWCNTs.[103]

SWCNTs have also been used within SMPs in order to achieve a multiresponse. In their work, Xiao et al. showed the beneficial characteristics of a pyrene-based SMP when 1−3 wt % SWCNTs was dispersed in a PCL copolymer in order to obtain a SMC that can be thermo-, electro-, or photoactivated.[104] Upon the application of a constant voltage of 50 V, the SMC heated to 65 °C in 20 s, which proved satisfactory during shape recovery.

Electrically assisted CNT dispersion has been used in order to align CNTs within polymer matrices. Electric fields have successfully been applied during curing of polymer networks in order to successfully orient the conductive fillers in the direction of the current.[105] Martin et al. showed that AC electrical fields achieve more linearly oriented conductive fillers in comparison to DC electric fields, which results in a more inhomogeneous and branched dispersion.[106] These highly oriented nanocomposites overcome the percolation threshold at lower concentrations and show anisotropic electrical properties as well as decent optical transparency. Yu et al. created a SMC with embedded CB where the chained CNT dispersion was shown to decrease the electrical resistivity by

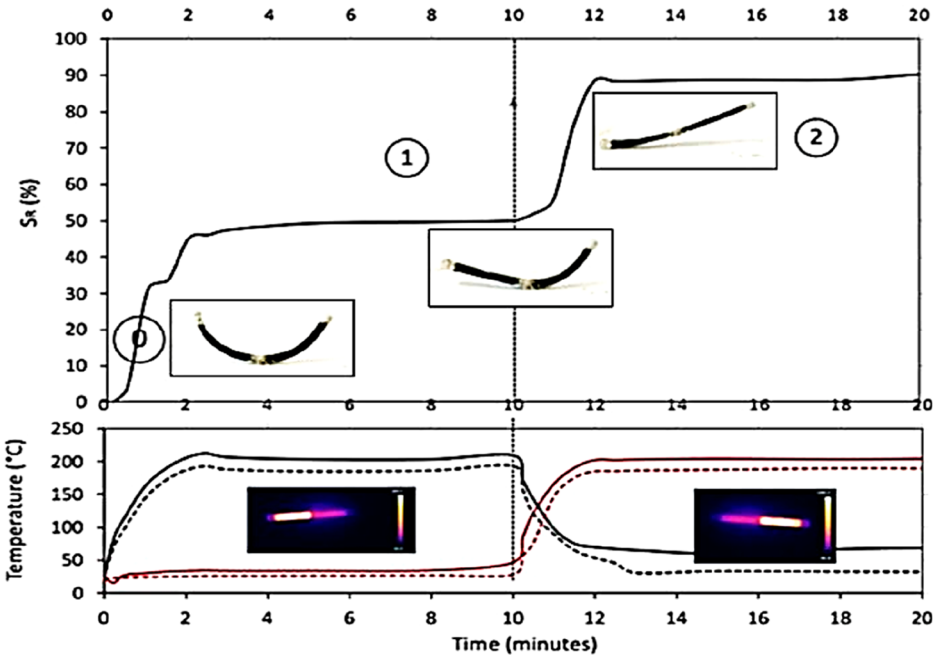

Figure 7. Sequential shape recovery due to selective resistive heating of a shape memory composite stripe. Three electrodes are painted on the surface of the SMC and are located on the right and left tips and another in between. The regions that heat up depend on which electrodes are used for injecting the electric current. During the first 10 min the current is injected between the central and left electrodes and during the last 10 min between the central and right electrodes (reprinted from ref 102, with permission of Elsevier.)

https://doi.org/10.1021/acsomega.2c05930
ACS Omega XXXX, XXX, XXX−XXX

over 1 order of magnitude in comparison to the SMC with a randomly oriented distribution.[107]

3.1.3. Carbon Nanofiber. Carbon nanofibers (CNFs) have been reported as a cheaper alternative to CNTs to improve the electrical conductivity of a PCL shape memory polymer matrix.[108] The resulting electrical resistivity for a concentration of 10 wt % is reported to be double that of the composites with CNTs at the same concentration. In an attempt to further decrease the electrical resistivity with carbon nanofibers, another PCL-based composite using carbon fiber felt (CFF) was reported by Gong et al. to have an electrical resistivity of 0.78 Ω m at a lower concentration of 3.6 wt % CFF.[109]

3.1.4. Graphene. Graphene is another carbonaceous filler that is used in SMCs due to its excellent electrical and thermal conductivities. To facilitate a homogeneous dispersion within the SMP, graphene oxide (GO) and reduced graphene oxide (rGO) are usually utilized. Wang et al. investigated an epoxy nanocomposite incorporating rGO nanopaper that underwent complete shape recovery within 5 s by applying a low electric voltage of 6 V.[110] The 2W-SM effect has also been shown in a shape memory polyurethane filled with graphene nanosheets.[111] The work demonstrates the 2W-SM effect that can be electrically triggered for higher concentrations of 4 and 8 wt %, which resulted in SMC samples with electrical resistivities of 5.49 and 1.17 Ω m, respectively. During the conventional 1W-SM effect, this SMC shows improved shape memory characteristics, amounting to 93% shape fixity and 95% shape recovery at concentrations of 2 wt %. The investigation reported in this work also shows a better thermal stability of the resulting composite, with higher melting and crystallization temperatures after the addition of the conductive filler. A similar trend can be found in amorphous shape memory nanocomposites: an increased glass transition temperature is observed in amorphous shape memory nanocomposites by the addition of graphene[112] with respect to the pristine polymer. After a certain concentration of graphene within the SMP, the glass transition temperature and the shape memory properties start to deteriorate due to poor dispersion and aggregation of the fillers.[113] This investigation reported an optimized concentration of 1.5 phr of GO inside the polyurethane SMP. The same research group also examined the electroactive shape memory performance of the SMCs.[114] The composites with 1.5 phr rGO could not be heated with their available setup due to a relatively high electrical resistivity on the order of 15 Ω m. However, the electrical resistivity of their SMC with 2.5 phr decreased to 0.4 Ω m. The values of the electrical resistivity reported here are calculated from the data presented in ref 114. Shape recovery of this SMC was obtained by applying 50 V and reaching a temperature of 64 °C after 90 s. A much faster electric shape recovery was reported in a poly(vinyl acetate) SMC with 4.5 wt % rGO.[115] The resulting SMC has an electrical resistivity 0.037 Ω m. By applying 70 V, full shape recovery was demonstrated to happen within 2.5 s. Similarly, graphene-filled PCL has shown to achieve satisfactory electrical resistivities for slightly higher concentrations: i.e. 0.09 Ω m for 7 wt % reduced graphene oxide.[116] Graphene−MWCNT hybrids have also been reported in a PCL matrix.[117,118] Although the electrical resistivity using such hybrid conductive fillers may be somewhat smaller than those reported for MWCNT-filled SMCs, as the price of graphene (or SWCNTs) is much greater than that of MWCNTs for a limited improvement in the electrical characteristics, limits graphene competitiveness.[119]

Concerning the effect of graphene in the mechanical properties of the resulting SMPs, Chen et al. reported increases of 64% and 71% in the tensile strength and elastic modulus by adding 3 wt % of rGO in a shape memory epoxy matrix.[120] It has been widely observed in the literature that the addition of high concentrations of graphene-based fillers increases the tensile strength of the resulting composite. The improved load-bearing capabilities usually come at the cost of worse shape memory characteristics due to the agglomeration of graphene at high concentrations. Interestingly, Zhang et al. proposed a method of functionalizing GO in order to produce a SMC that has both high load-bearing capabilities with an elastic modulus of 456.7 MPa and an excellent shape recovery of 100%.[121]

For further information on graphene-filled shape memory polymers, the reader can consult a recently written comprehensive review on this topic written by Kausar[122] and the references therein.

3.2. Ferromagnetic Nanofillers. One of the most used magnetic fillers in SMCs is Fe_3O_4 because of its biocompatibility and nontoxicity, which enables their utilization for medical purposes. Other magnetic fillers that have been reported in the literature are particles of Fe_2O_3, Ni, NiZn, NdFeB, or NiMnGa. Examples of materials with these and other fillers can be found in a recent review written by van Vilsteren, Yarmand, and Ghodrat.[123] Even though some SMCs contain nickel-based magnetic nanoparticles,[124−126] no reference was found where these particles were used for the magnetic heating of the smart composites, with the exception of NiZn ferrite nanoparticles. For instance, Buckley et al. used 10 vol % NiZn ferrite nanoparticles dispersed in their SMP and achieved a temperature increase of 11 °C after 40 s in a 545 A m^{-1} magnetic field at 12.2 MHz.[127] The fact that nickel nanoparticles are not or are rarely used in magnetoactive SMCs may be due to the lower heating efficiency of the polymer with Ni than with other nanoparticles such as iron or magnetite.[128] Furthermore, the use of nickel nanoparticles may be limited in magnetic heating due to the complex synthesis,[129] carcinogenic effects,[130] and the unavoidable formation of oxide layers on the nickel nanoparticles, which is shown to detrimentally affect the magnetic heating ability.[131] By adding polymer coatings to fight these drawbacks, the heating efficiency of nickel nanoparticles is dramatically decreased.[129]

Conventionally, magnetic particles are incorporated in the SMP matrix by physical blending. Due to van der Waals and magnetic forces, the unmodified magnetic particles tend to aggregate. This, together with the weak compatibility between the particles and the matrix, results in unsatisfactory mechanical and shape memory properties.[132] In order to reduce the agglomeration of particles and improve the properties of the composite, several techniques have proven satisfactory, such as filler surface modification,[132] chemical modification of the polymer matrix,[133] or mechanical ultrasonication.[134]

The shape memory characteristics of magnetosensitive SMCs has been investigated in terms of the heating mechanism.[135] It was found that the shape fixity ratio was higher in magnetosensitive SMCs when they were activated with magnetic heating rather than activated with conventional heating. The shape recovery ratio at a given magnetic field intensity, on the other hand, depends on the concentration of the magnetic fillers. It is higher for conventional heating when a low amount of magnetic fillers is dispersed. Nevertheless, after a certain threshold is attained, magnetic heating also results in a higher shape recovery ratio than conventional heating. Moreover, a few years later, the same research group investigated different parameters that have an influence on the temperature that can be reached with

https://doi.org/10.1021/acsomega.2c05930
ACS Omega XXXX, XXX, XXX−XXX

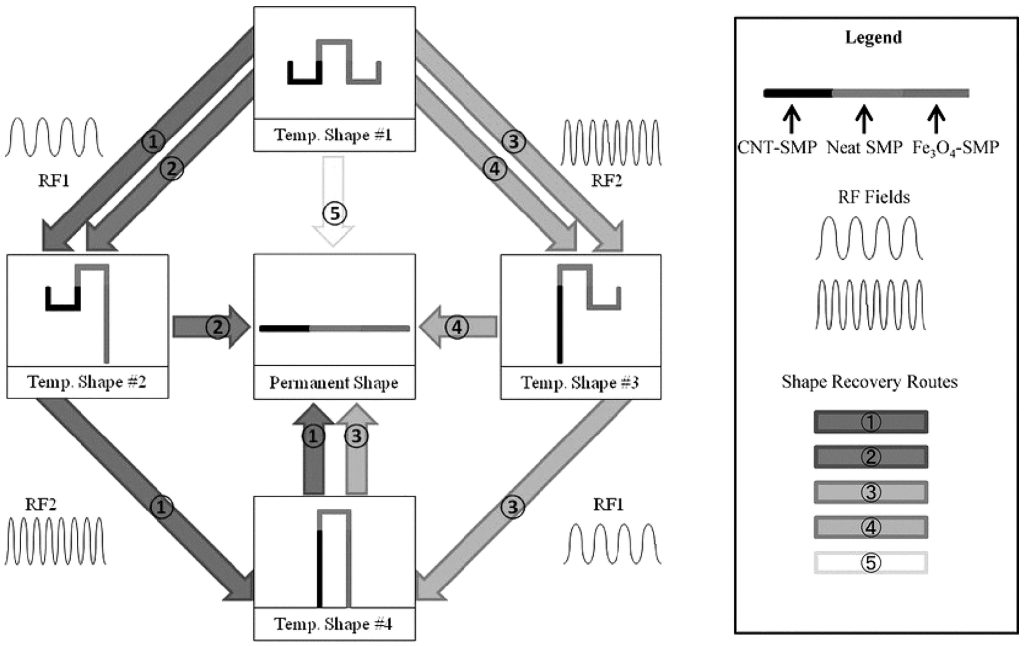

Figure 8. Illustration of the five shape recovery routes that can be followed from temporary Shape #1 to the permanent flat shape of a SMC with three different regions: CNT-SMP that can be activated with inductive heating at 13.56 MHz, neat SMP that can be activated with conventional heating, and Fe_3O_4-SMP that can be activated with inductive heating at 256 kHz. (Reproduced from ref 137 with permission of John Wiley and Sons. Copyright 2011 Wiley-VCH.)

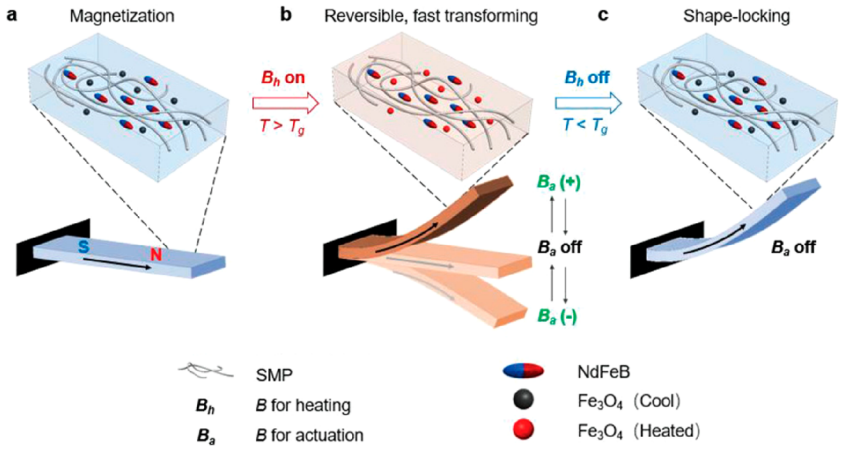

Figure 9. Principle of operation of a multishape magnetosensitive SMC with embedded NdFeB and Fe_3O_4 particles. (a) Illustration of magnetization and composition. (b) The SMC is heated by the application of a high-frequency AC magnetic field B_h above the glass transition of the SMP. Deformation and actuation can be achieved by a DC (or low-frequency AC) magnetic field B_a. (c) Shape fixity can be achieved by removing B_h while keeping the desired B_a. (Reproduced from ref 141, with permission of John Wiley and Sons. Copyright 2019 Wiley-VCH.)

inductive heating on a biodegradable multiblock copolymer filled with Fe_3O_4.[136] The magnetic field intensity H was varied between 7 and 30 kA m^{-1} (corresponding to $\mu_0 H$ = 8.8−37.7 mT, where μ_0 is the magnetic permeability of free space) with frequencies between 253 and 732 kHz. They found that increasing the nanoparticle concentration and the magnetic field strength resulted in higher temperatures. They also studied the influence of the surrounding environment, leading to a lower steady-state temperature in distilled water than in air, and a considerably slower heating phenomenon when the material was submerged in a saline solution. Furthermore, the composition of the magnetic nanoparticles and their distribution within the polymer matrix were investigated. They found that, with a homogeneous distribution of 10 wt % of Fe_3O_4 nanoparticles, the mechanical properties of the composite were not dramatically different from those of the pristine SMP, while observing and improvement in its shape fixity by 7% and the shape recovery ratio by >2% on the third shape memory cycle.

An SMC with multiple fillers was fabricated by He et al.[137] The conformation of the composite structure allowed for remotely and selectively triggering the shape recovery in specific regions in order to obtain different shapes. Their composite structure was divided into three regions with different compositions, as illustrated in Figure 8: on the right an epoxy SMP filled with 5 wt % Fe_3O_4 nanoparticles, on the center neat epoxy SMP, and on the left the epoxy SMP filled with 0.4 wt % CNTs. The selective triggering of the shape memory effect is due to a frequency effect: the region with Fe_3O_4 heats up by a magnetic field at 296 kHz, and the region with CNTs heats up by a magnetic field at 13.56 MHz. Among the plausible mechanisms

https://doi.org/10.1021/acsomega.2c05930
ACS Omega XXXX, XXX, XXX−XXX

responsible for the heating of the CNT-filled region when the material is subjected to a high-frequency magnetic field, one could be the presence of ferromagnetic metal impurities in the CNTs as a result of their manufacturing.[138−140] After the shape programming process where the permanent (straight) shape is heated past the T_{trans} and deformed into the temporary shape (temporary shape #1), the recovery back toward the permanent shape can follow five different recovery routes with five total intermediate temporary shapes. Figure 8 illustrates each recovery path with a different arrow color (in gray values) together with a sketch of the required frequency of activation. The last step of each route toward the flat permanent shape needs to be achieved with conventional heating of the composite since the neat SMP central area does not contain any filler.

SMCs with multiple ferromagnetic particles have also been produced in order to achieve a functional 2W-SM behavior.[141] In this investigation, Fe_3O_4 and magnetized NdFeB particles were dispersed in an acrylate-based SMP. The Fe_3O_4 particles, with an average size of 30 μm, were heated by hysteresis loss with a high-frequency magnetic field of 10 mT at 60 kHz. The NdFeB particles, characterized by having huge coercivity, do not contribute to the heating due the small magnitude of the magnetic field. Instead, the NdFeB particles are used to generate a magnetic torque and induce a shape change when they are subjected to a DC magnetic field of 30 mT. As depicted in Figure 9, first the AC magnetic field B_h is applied onto the structure in order to heat up the material. When the T_{trans} is surpassed, the DC magnetic field B_a will cause the cantilever beam to bend. The new temporary shape can be fixed by removing the AC magnetic field while keeping the DC field. Otherwise, the material can be used as an actuator by keeping the AC magnetic field and varying the sign of the DC magnetic field at a low frequency (0.25 Hz), hence creating a reversible bending transformation of the beam. Besides the interesting potential applications and versatility of shape morphing and actuation of this material, the authors also proved the excellent shape memory characteristics, amounting to a shape fixity ratio of 95% and complete shape recovery.

Even though magnetic particles are normally embedded inside SMPs to enable magnetic heating of the resulting composite, some research groups have used them as means of increasing the electrical conductivity of the polymer matrix and heated the resulting composite with the Joule effect by injecting an electric current. Leng and co-workers have produced a polyurethane SMP with dispersed Ni powder. They produced aligned Ni chains by using a magnetic field during the curing of the SMP.[142] The aided alignment of the magnetic nanoparticles helped to reduce the electric resistivity to <0.1 Ω m for 20 vol % of Ni powder. Resistive heating of up to 55 °C was shown when applying 6 V.

3.3. Other Fillers. Noble metals in the form of nanoparticles have attracted interest as fillers of SMPs in order to achieve multistimuli SMCs. This is due to their photothermal effect, where they absorb light at certain wavelengths from UV to near-IR and convert it into thermal energy. In their investigation, Mishra and Tracy created two similar SMCs filled with either gold nanospheres or gold nanorods, and they were able to selectively trigger the shape memory effect depending on the wavelength of light used: 530 nm for the nanospheres and 860 nm for the nanorods.[143] Other noble metals that have been used to photothermally activate SMCs are platinum[144] and silver nanoparticles.[145] Besides nanoparticles of noble metals, metallic ions have been incorporated as fillers in SMCs to activate the shape memory effect using light in the near-IR. Bai et al. reported a composite made by cross-linking poly(acrylic acid) and poly(vinyl alcohol) with different metallic ions.[146] They looked into Cu^{2+}, Cd^{2+}, Cr^{2+}, Al^{3+}, and ions of ferromagnetic materials (Fe^{3+}, Co^{2+} and Ni^{2+}).

The SMCs containing polypyrrole (Ppy) can take advantage of the electrical conductivity of the particles for electrically triggering the shape memory effect.[147,148] Moreover, Ppy-SMP composites are also shown to exhibit an excellent photothermal performance. Thus, these SMCs are multistimuli. There are many other fillers that have been used in shape memory polymer composites in order to improve mechanical, thermal, and electrical properties or to obtain multistimuli materials. For example, shape memory alloys have been embedded in SMPs in the form of wires[149] or particules.[80] Silicon carbide has been used due to its temperature stability and good microwave absorption that allows the SMM to be activated through multiple stimuli.[150] Oxides of tungsten, silicon, or aluminum have been incorporated in order to improve the mechanical properties of SMC foams for medical devices.[151] Other electroactive polymers have been blended with SMPs,[152] liquid metals have been used to fill the SMP and achieve electro-activation,[153] and fillers such as cellulose nanocrystals[154] or nanoparticules of mineral silicates[151] have been used to reinforce the SMP but do not enable electro- or magnetoactivation.

After this overview of fillers in SMCs, the reader can proceed to the Appendix, which lists some of the many existing references on electro- and magnetosensitive SMCs, together with the activation mechanism and general characteristics of the materials reported.

4. APPLICATIONS

In view of the highly tailorable material properties of SMCs together with the excellent shape memory properties and possible and versatile multistimuli activation, SMCs are used (or intend to be used) in many areas of research and industry. In this section, a few applications of shape memory composites are described, paying special attention to those that can be electrically activated.

4.1. Biomedical Industry. Within the biomedical industry, shape memory polymers have attracted a great deal of attention. Most of the applications in this field use conventional heating of SMPs[4] or heating with magnetic fields of SMCs with magnetic nanofillers. A composite made from a poly(lactic acid) SMP with dispersed 10 wt % Fe_3O_4 nanoparticles was used in 4D printing in order to fabricate prototypes of shape memory heart occluders for the treatment of congenital heart diseases.[155] A similar SMC was used for conceiving a tracheal scaffold.[156,157] The composite, with 15 wt % Fe_3O_4, is to be implanted as a flat surface and, under the influence of an AC magnetic field of 4 kA m^{-1} at 30 kHz, it curls to form a tube within 35 s, as shown in Figure 10a. Moreover, the same research group also reported on the feasibility of this SMC to create different designs of bioinspired scaffolds to be applied for bone repair and regeneration.[158] One of the proposed structural designs is shown in Figure 10b, where the magnetic activation (4 kA m^{-1} at 30 kHz) expands the SMC scaffolds within 15 s. As an additional example, magnetoactive SMCs have also been conceived in the biomedical field to apply in drug delivery[159] or as intravascular stents.[160,161]

Electroactive SMCs have also been found to be the material of choice for biomedical applications in the literature. For example, a porous SMP foam with homogeneously dispersed CNTs has been fabricated for the potential treatment of intracranial

https://doi.org/10.1021/acsomega.2c05930
ACS Omega XXXX, XXX, XXX−XXX

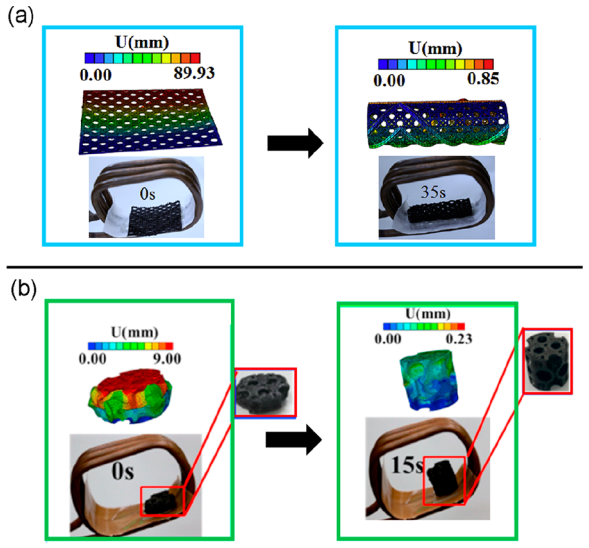

Figure 10. 4D printed poly(lactic acid) SMP with embedded Fe_3O_4 composites actuated by a magnetic field for the conception of (a) tracheal scaffolds (reprinted from ref 156, with permission from Elsevier) and (b) porous bone tissue scaffolds (reprinted from ref 158. with permission from Elsevier.)

aneurysms by implantation through a catheter (Figure 11a) and subsequent expansion of the foam in order to fill the aneurysm,

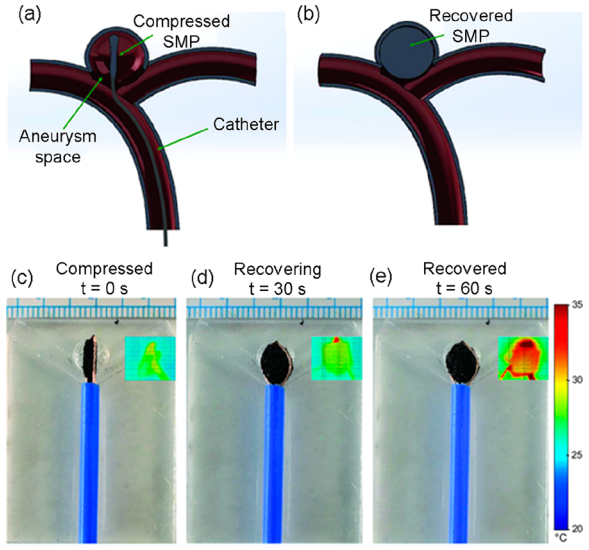

Figure 11. Illustration of the treatment of aneurysms by filling them with a SMC. (a) Compressed SMC foam being placed in a saccular aneurysm via a catheter. (b) Recovered expanded shape of the SMC filling the aneurysm space. Demonstration of the prototype for the treatment of aneurysms of a SMC with 1 wt % CNTs at (c) 0 s, (d) 30 s, and (e) 60 s after the injection of an electric current (1 A). (Reproduced from ref 162 with permission of John Wiley and Sons. Copyright 2021 Wiley-VCH).

as illustrated in Figure 11b.[162] Thanks to the incorporation of the CNTs, X-ray imaging can be used during the implantation procedure to visualize the path of the SMP foam. The researchers used a foam with 1 wt % CNTs and investigated the steady-state temperature reached due to the injection of a constant current. After compressing the foam to 60% of its initial volume, the authors triggered shape recovery to the expanded foam in less than 1 min by injecting 1 A (Figure 11c–e), demonstrating in this way the potential of the SMC in the treatment of aneurysms. A similar investigation was reported in their previous work with 0.005 g mol^{-1} CNTs.[163] The applied deformation toward the temporary shape is a compression of more than 50%. Complete electrically triggered shape recovery toward the expanded permanent shape happened within 2 min at 0.2 A and reached a maximum temperature of 46.8 °C, preventing neighboring tissue damage.

4.2. Aerospace Industry. Within the aerospace field, self-deployable structures have been reported using magnetoactive SMCs. A reconfigurable morphing antenna was reported to be heated in an AC magnetic field of 40 mT at 60 kHz to be used as a self-deployable structure or as a structure with variable resonant frequencies.[141] Regarding electroactive SMCs, Paik et al. fabricated a SMC made of polyurethane with 7 wt % MWCNTs by *in situ* polymerization. The electrical resistivity of the SMC was around 0.8 Ω m. The SMC was applied in a microaerial vehicle to actuate the control surface (rudder).[164] When an electric current was injected in the SMC, it shrunk and produced a 30° angle deflection. Unfortunately, because this was a 1W-SM effect, subsequent shape memory programming was be needed for further deflection of the control surface, which is not compatible with realistic flight control. More recently, a hybrid shape memory composite actuator has been developed as a laminate composed of SMA wires and SMP filled with nichrome for morphing flap flight.[165] Resistive heating was induced in the composite structure by injecting a current of 0.7 A in the SMA wires and of 0.4 A in the SMP–nichrome composite. The authors used this composite for the morphing of the trailing edge of the wings of an unmanned aerial vehicle, resulting in deformation angles between 32 and 39°, as shown in Figure 12. The flapping of the trailing edge proved to create an extra lift force on the wing while decreasing the drag.

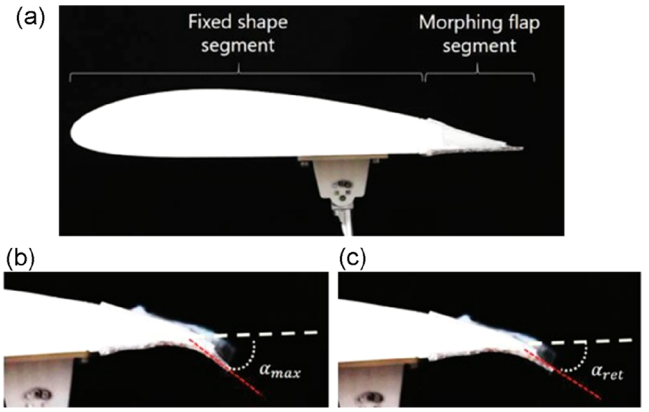

Figure 12. (a) Wing of an unmanned aerial vehicle with a morphing flap at the trailing edge capable of changing the deformation angle between (b) 39° and (c) 32°. The actuation mechanism is through resistive heating of both the SMA wires and the SMP–nichrome composite. (Reprinted from ref 165, with permission from Elsevier.)

4.3. Soft Robotics. Using a magnetoactive SMC made of poly(aryl ether ketone) with dispersed Fe_3O_4 nanoparticles, Yang et al. showed the diversity of potential applications of their composite exhibiting a remotely and magnetically triggered 1W-SM effect.[166] Their layered-film nanocomposite with 15 wt % magnetic nanoparticles was subjected to an AC magnetic field of 27.9 kHz for 50 s. They fabricated a ball launcher that propelled

https://doi.org/10.1021/acsomega.2c05930
ACS Omega XXXX, XXX, XXX–XXX

a ball forward by triggering the shape recovery with the AC magnetic field. Moreover, they showed the morphing abilities of their composite material with flower-shaped and plane-shaped geometries that unfolded back to a flat position with the application of the magnetic field. Other soft robotic applications were envisioned by, for instance, Cohn et al., using their SMC of polycaprolactone dimethacrylate with 5 wt % of Fe_3O_4 nanoparticles.[167] In their published work, they showed the morphing of several structures when the material was subjected to a magnetic field (4 kA m^{-1} at 375 kHz) such as a self-deployable honeycomb cylinder or a spider web and the folding of a spiral. They investigated rolling and gripping movements using their SMC.

A crawling robot was reported by Peng et al.[168] In this work, they used a double layer of a 3D porous CNT sponge SMP to create a nanocomposite that was able to undergo a 2W-SM effect when it was subjected to resistive heating. The CNT loading inside the composite was of 1.08 wt %, which resulted in an electrical resistivity of about 0.007 Ω m. They recreated an inchworm locomotion by applying voltages between 2 and 8 V. The inchworm-like robot is able to travel 1.2 cm in 10 min. Xu et al. produced another SMC made of poly(ethylene-*co*-octene) filled with CNTs to achieve a composite was is able to undergo a stress-free 2W-SM effect with a fast response when it was subjected to either low voltages (<36 V) or infrared light (250 mW cm^{-2}).[48] In this work, they built an electroactive gripper and a photoactive crawling robot. The gripper, shown in Figure 13, was formed in a C shape. At room temperature, the opening

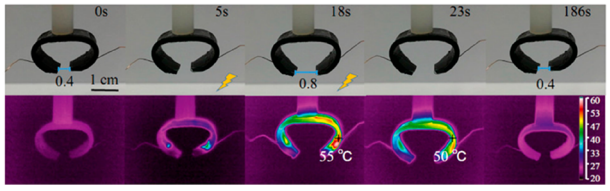

Figure 13. (a) Photographs and (b) IR thermal images of the SMC electroactive gripper. (Adapted with permission from ref 48. Copyright 2019 American Chemical Society.)

of both tips of the C shape was 0.4 cm. Upon the application of 36 V, the temperature of the composite increased to 55 °C and the shape changed by increasing the aperture to 0.8 cm in 18 s. When the material was cooled once again, the original opening of 0.4 cm was recovered after 168 s. They showed the lifting capabilities of this gripper by lifting 15 nuts (69.09 g). In their most recent work, Xu et al. also reported a high-temperature warning robot that was made possible by the addition of paraffin wax into the composite.[169] They hot-pressed the SMC layer with sandpaper to make the surface uneven, and they stacked two uneven-surfaced layers together. At high temperature, the stiffness of the SMC decreased and the surface roughness disappeared, leaning to a better contact between both layers that could be monitored thanks to a change of electrical resistivity across the layers of more than 2 orders of magnitude.

Other works have also exploited the weight-lifting and 2W-SM and multiple shape capabilities of SMCs. Xu et al. used a poly(ethylene-*co*-vinyl acetate) filled with CNTs that was activated with a voltage.[170] Instead of using the SMC as the grip, they mounted it in a setup that permitted the opening and closing of a mechanical grip due to the elongation and contraction of the SMC during its 2W-SM effect. Furthermore, Hu et al. built a device with a magnetoresistive triple SMC that was capable of displaying text in Braille and self-refresh in order to potentially apply it as a Braille e-book.[171]

4.4. 4D Printing. Within 4D printing, Dong et al. investigated several applications in poly(lactic acid) filled with 8 wt % CNTs.[172] They demonstrated the fast shape recovery (<44 s) of pyramid-, diamond-, and crown-shaped printed structures when they were subjected to voltages in the range 20−35 V. Interestingly, they also developed a multisegment self-deployable rectangular structure that can be selectively deployed in three sections. Each section was actuated with 25 V in order to reach a temperature >70 °C. Moreover, they also developed an external stent that can be implanted in an extended unfolded shape outside of the body part. By applying 20 V, the stent shrinks and bends within 60 s.

4.5. Self-Healing. Self-healing of structures is another popular application that has been investigated in the scope of electrically and magnetically triggered shape memory composites. This property can be used in a plethora of applications in order to self-repair surfaces and structures that have suffered from impact or fatigue, thus prolonging the life of the structure and delaying disposal. An example of this kind of composite was reported by Ren et al.[173] It consisted of a polycaprolactone/thermoplastic polyurethane SMP with 2−6 wt % CNTs that exhibited fixity and shape recovery ratios of 96% and 94%, respectively. They reported excellent electrically triggered healing efficiencies of the composites ranging from 94.79% to 96.15%. Furthermore, comprehensive reviews on electroactive[174] and magnetoactive[175] self-healable nanocomposites have been recently published, where other examples of shape memory self-healable materials can be found.

Besides the applications that have already been reported in the literature, the interesting properties of electro- and magneto-active SMCs make these materials excellent candidates for other prospective applications such as artificial muscles, self-deploying antennae and solar arrays, dental fixtures, self-foldable devices, and many more.[176,177]

5. CONCLUSIONS AND FUTURE HORIZONS

Bearing in mind all the information and the numerous references cited in this review, it is not surprising to say that SMPs and SMCs have attracted a great deal of attention and interest from researchers and the industry. Even though shape memory materials have been investigated for years, there are probably many things to discover, many properties to keep enhancing, and many applications to be conceived.

Considering the extensive literature review performed, some prospective future directions in the research field of shape memory polymer and their composites are listed here below.

(i) High importance has been given in recent research to minimize the time during shape recovery of SMCs for their application as actuators. This trend will likely continue in order to obtain faster SMC actuators. Besides the ability to achieve a fast recovery time, a variable time scale or even a fast interruption of the shape recovery may be desirable for some applications, notably in the biomedical field.

(ii) Materials with a tunable transition temperature are highly desirable, but further investigation is needed in order to do so accurately and repetitively. Furthermore, broad transitions may lead to multiple intermediate temporary shapes during a slow shape recovery. The accurate characterization, description, and prediction of these

https://doi.org/10.1021/acsomega.2c05930
ACS Omega XXXX, XXX, XXX−XXX

Table 1. Compilation of References of Shape Memory Composites Activated with an Electric or Magnetic Field

SMP	filler	ς	ρ_e (Ω m)	activation	activation magnitude	T reached (°C)	t_R (s)	comments	ref
PCL	MWCNT	3 wt %	0.15−0.6	electrical	controlled resistive heating (0.6−15.7 mA)	60	130	1W-SM and 2W-SM effects; R_F > 96.7% and R_R > 88.9%; variable electric current to achieve constant temperature and constant heating and cooling rates; nonlinear evolution of ρ_e within shape memory cycle	101
PU	MWCNT + Fe_3O_4	30 wt % Fe_3O_4 + 0.25−1 wt % MWCNT		magnetic	29.7 kA/m at 45 kHz	>45	60	R_R >95%	178
PU/SM-PU	CB	1−5 wt %	5×10^{-2} Ω m for 5 wt %; 10^{-3} Ω m for 3 wt %	electrical	100 V		25	2W-SM; R_R 99.8%	179
PU	MWCNT	5 wt %	∼1 Ω m	electrical	60 V	100	10		180
EP	MWCNT	0.2 wt %	1−10 Ω m	electrical	126−265 V	200−250	<300	sequential recovery	102
EP	MWCNT	30 wt %	47 Ω m	electrical	12 V	>55	22		98
EP	rGO	0.5 wt %	0.025 Ω m	electrical	10 V	>100	10	R_F = 95% and R_R = 98%; electrical recovery	181
PLA/PU	MWCNT and CF	6 wt %		electrical	10 V	>70	25	R_R = 94%; negative Poisson ratio	182
PVAl	MWCNT	5−30 wt %	0.52 Ω m for 30 wt %	electrical	45−120 V	>74	35		183
PCL	MWCNT coated Fe_3O_4			magnetic	6.8 kA/m at 20 kHz	T increase of 17.2	120	alignment of Fe_3O_4-coated MWCNT due to magnetic field 0.2 T; increase of elastic modulus by almost 100% but reduction of max elongation	184
PCL	MWCNT	3 wt %	0.05 Ω m	electrical	0.1 W	∼50		analytical, numerical, and experimental investigation	100
BR	MWCNT and CB	0−15 phr MWCNT or 0−30 phr CB	10^{-2} Ω m for 15 phr CNT or 30 phr CB	electrical	50 V	110 after 15 min at 50 V	900	lower ρ_e and higher R_F and R_R for CNT than CB	87
PU	Fe_3O_4	0−9 wt %		magnetic	250 A/m at 20 kHz	>52	35	R_R decrease with ς, slight R_F increase with ς	185
PBS−PEG	CNT	0.2−1 wt %	7.05 Ω m for 1 wt %	electrical	20−120 V	85 at 70 V for 1 wt %	55	CNT reduced ductility	186
PU	CNF	1−7 wt %	560 Ω m for 7 wt %	electrical	100−300 V	25−55		χ_c, R_F decrease with ς of CNF; elastic modulus increase with CNF ς	187
PU	CNT	3 wt %	0.037 Ω m	electrical	50 V	>40	40	different preparation techniques and effect of dispersion and electrical properties	93
PU	G sheet	1−8 wt %	1.17 Ω m for 8 wt %	electrical	65−80 V	>70	8	2W-SM; study mechanical properties; R_F = 95%; R_R = 93%	111
PU	CNT	4 wt %		electrical	40 V	100 cross-linked CNT	50	CNT covalently bonded to PU; increase R_R and R_F for cross-linked CNT (>10%)	92
PU	rGO	0−2.5 phr	0.4 Ω m for 2.5 phr	electrical	50 V	64 for 2.5 phr	120	T_g and mechanical properties increase with ς; ductility increase with cycles; R_R decreases with ς	114
EOC	CB	0−38 wt %	0.08 Ω m for 17 wt %	electrical	5−15 V for 17 wt %	40−160	60	two different CB fillers; lower R_R for higher ς	85
PU	rGO + Fe_3O_4 and γ-Fe_2O_3	3 wt % GO + 7 wt % Fe_3O_4		magnetic	287 kHz with 300A in coil	70 for mixture, 60 for hybrid	60	Young modulus doubled from hybrid to only Fe_3O_4	188
PU	Ni powder chains	0−20 vol%	0.005−0.01 Ω m for 20%, 10^4 for 4%	electrical	6 V	55	90	alignment magnetic field; decrease T_g with ς	142
PU	CB with and without 0.5 vol% Ni	4−10% CB	0.1 Ω m for 10% CB + chained 0.5% Ni	electrical	30 V	80	120	ρ_e increases with number of cycles	189
PVAl	CNT and G	20 phr GO and 4−16 phr CNT	0.1 Ω m for 20 GO + 16 CNT	electrical	60 V	100 max (normally 60)	120	ρ_e decreases with bending angle	190
PS	CNT	1.47−7.02 wt %	0.01 Ω m for 7.02 wt %	electrical	35 V	>85	80	$R_R \approx$ 100%	96
PU	GNP	1−3%	4 Ω m for 3% GNP	electrical	75 V	100 for 3%	60	χ_c, elastic modulus, R_F and R_R increase with ς; strength, T_g, and T_m decrease with ς	191
EP	Ag decorated rGO and CF mat	2−4 wt % rGO and 11.6% CF	2.3×10^3 Ω m	electrical	8.6 V	100	36	R_R = 99%	192

https://doi.org/10.1021/acsomega.2c05930
ACS Omega XXXX, XXX, XXX−XXX

Table 1. continued

SMP	filler	ς	ρ_e (Ω m)	activation	activation magnitude	T reached (°C)	t_R (s)	comments	ref
PS	MWCNT nanopaper	1.47−7.02 wt %	0.008 Ω m for 7.02 wt %	electrical	0.6 A	>62	300	R_R = 98%	95
EP	CNF	9.18 wt %?	0.03 Ω m	electrical	10−20 V	>50	2.1	increase elastic modulus above T_g, increase κ	193
PU	MWCNT	3−7 wt %	12 Ω m for 3 wt %	electrical	40 V	>70 in 10 s	9	Young modulus increase by 50%; R_R > 98%; T_c increase with ς	194
PU	Fe_3O_4	0−10 wt %		magnetic	30 kA/m at 258 kHz	70 at 150 s 12.5 kA/m 258 kHz	22	magnetic heating depends on geometry; for high ς, R_F and R_R higher for magnetic actuation	135
PK BMI	MWCNT	8 wt %	∼ 0.06 Ω m	electrical	20−50 V	40−140		R_R = 90% by 40 V; self-healing	195
PU	MWCNT	3−10%	0.9 Ω m	electrical	9.5 mA	32			164
PU	GO	0−20 phr	>7 × 10^2 Ω m	electrical	100−200 V	<60			196
EP	Fe_3O_4 coated with oelic acid	1.5−8 wt %		magnetic	30 mT at 293 kHz	T increase of +25	60		133
PPC/PLA	MWCNT	1−3 phr	0.1 Ω m for 3 phr	electrical	20−30 V	130 max for PPC/PLA (50/50) 3 phr at 30 V	30	max tensile strength and strain at break increased with ς at room temperature; At 50 °C strength decrease with concentration; R_R = 97%	197
PLA/PU (70/30)	CB	0−8 phr	∼0.4 Ω m for 8 phr	electrical	30 V	98 for 8 phr	80	R_F = 90%; R_R increase from 59% to 85.9% for 8 phr CB; conductivity ∼1 order of magnitude higher for PLA/PU(70/30) than for PLA	198
PU	CF/PU yarn fabric	10.9% CF	1 × 10^{-3} Ω m	electrical	6 V	87	80	R_R = 99.3%; applications of deployable structure	82
PEVA	CNF	0−15 wt %	0.204 Ω m for 15 wt %; 5 × 10^9 Ω m for 3 wt %	electrical	60 V	100 after 25 s		2W-SM; R_R decreases with ς	199
PU/PCL	modified MWCNT	2−10 wt %	1 Ω m for 10 wt %; 10^2 Ω m for 4 wt %	electrical	40 V	>50	15	T_g of PLA increase with ς; $T_g$of PU decrease with ς; $T_c$decrease with ς	200
PU/PVDF (90/10)	modified MWCNT	0−10 wt %	50 Ω m for 10 wt % pristine CNT; 4 Ω m for 10 wt % modified CNT	electrical	40 V	T rise of +40	15	κ × 4 by adding 10 wt % MWCNT; increase 10% tensile strength and decrease 100% elongation at break for surface-modified MWCNT than pristine; R_R decrease with cycles faster for modified than pristine CNT	94
PU	Fe_3O_4	0−40 vol%	10^6 Ω m for 40 vol%	magnetic	4.4 kA/m at 50 Hz	50	1200	electric percolation at 30 wt %; C_p decrease with ς; κ increased by 0.4 for 40 vol %	201
PEVA and PU	FE_2O_3	0−13.6 wt %		magnetic	15−23 kA/m	100 for PEVA; 108 for PU			202
PDL	Fe_3O_4	5−11 wt %		magnetic	7−30 kA/m at 258 kHz	100	180	decreased R_F (95% to 90%) and increased R_R (95% to 97%) for increased ς	203
EP	CB	0−10 wt %	200 Ω m for 10 wt %	electrical	3.5 W constant power	65	<200	ρ_e vs ε during elongation and recovery	204
PVA	GNP	1.5−4.5 wt %	0.04 Ω m for 4.5 wt %	electrical	50−70 V		2.5	elastic modulus increases by 1 order of magnitude from 0 to 4.5 wt %; T_g decrease with ς	115
PU	PPy	8−21%	0.105 Ω m	electrical	40 V	70	<30	T_m decrease with ς	205
PCL DMA	Fe_3O_4	2−12 wt %		magnetic	300 kHz, 5 W	43	20		206
PLA/PU (50/50)	CNT	1−5 wt %	0.33 Ω m for 5 wt %	electrical	50 V	50−70	<150	decrease R_R (13% smaller) in 5 wt %; faster shape recovery with electrical heating than conventional; higher R_R with electrical heating than conventional	207
EP	MWCNT nanopaper	40 wt %	3 × 10^{-3} Ω m	electrical	0−6 W	20−170	20	curing with resistive heating 105 °C after 40 s at 4.6 V; recovery at 76 °C	97
PE	CNF	0−11.6 vol%	0.1 Ω m for 11.6 vol%	electrical	1−40 V	100−110	100	T_c and elastic modulus increase with ς; T_m decrease with ς	208
PCL/MA (50/50)	MWCNT	0−10 phr	0.0384 Ω m	electrical	40 V	>70	56		90
PU	GNP			electrical	10−30 V	60 at 10 V	20		209
PCO/PE	MWCNT	8−15 vol%	0.0105 Ω m for 10 vol%	electrical	150 V	>120 after 2 min	90	triple SM effect; MWCNT dispersed in PCO; chemical cross-linking increases ρ_e due to agglomeration of fillers	210

https://doi.org/10.1021/acsomega.2c05930
ACS Omega XXXX, XXX, XXX−XXX

Table 1. continued

SMP	filler	ς	ρ_e (Ω m)	activation	activation magnitude	T reached (°C)	t_R (s)	comments	ref
SBS/ LLDPE	CB	0−25 wt %	1.08 Ω m for 1 wt % CB; 7.4×10^{-2} Ω m for 25 wt % CB	electrical	0−120 V		60	elongation at break decrease by 50% from 0 to 25 wt % CB; tensile strength increase by >50%; recovery at 40 V	211
EP	rGO		0.0027 Ω m	electrical	1−6 V	35−240	5	bending	110
PEVA/PCL	MWCNT	5 wt %	0.0205 Ω m	electrical	20 V	97	12	recovery at 30 V	212
PU	CNT	10 to 50 layers	22.96 Ω m	electrical	40 V	90	30	CNT layers at different locations; R_R = 100% at 40 V; localized and selective actuation	99
EP/CE	GNP	0.8−2.4%	11.3×10^{-2} Ω m for 2.4%	electrical	20−120 V		98	strength increased by 25% for 1.6 wt %; recovery at 60 V	213
EP	Ag-CF	5.4 wt %, 1.8 wt %	95.1 Ω m for 5.4 wt %; 1×10^6 Ω m for 1.8 wt %	electrical	60−120 V		60	R_F increase with ς; R_R decrease with ς	81
EP	MWCNT and CB	1.9 wt % total	2×10^5 Ω m for 0.8 wt % MWCNT	electrical	225 V	>80	570	R_R = 99%	214
PLA/PU (70/30)	MWCNT and CB	3−5 phr CB and 0−2 phr MWCNT	<0.1 Ω m for CB 5 phr and >1 phr MWCNT	electrical	30 V	70 °C	100	70 °C after 100 s for 3 phr CB and 1 phr CNT; R_R = 0	215
PPDO−PCL/PU	Fe_3O_4	0−10 wt %		magnetic	7−30 kA/m at 256−732 kHz	65			136
PMMA−PEG	Modified Fe_3O_4	1−5 wt %		magnetic	100 kHz, 8 kW	40.4	59	T rise 4 °C for-surface modified Fe_3O_4 than for pristine; R_F = 90%; R_R = 95%	216
PCL	modified MWCNT	0−9 wt %	20 Ω m for >7 wt %	electrical	50 V for 5 wt %	70	120	decrease R_R with ς	217
PCL-Py	SWCNT	2 wt %	3.6 Ω m	electrical	50 V	65	20	increase R_R with ς	104
MA-based thermoset	Fe_3O_4	0−2.5 wt %		magnetic	0.33 mT at 297 kHz	50	40		218
PS	MWCNT and CB	1 wt % MWCNT and 10−15 wt % CB	0.03 Ω m for CB. 0.025 Ω m for CB+CNT randomly oriented. 0.0075 Ω m for CB+CNT chained	electrical	25 V	>95	75	MWCNT in chains, reduction of ρ_e by more than 1 order of magnitude; ρ_e increases with number of shape memory cycles	107
acrylate	NdFeB and Fe_3O_4	15 vol % of each		magnetic	40 mT at 60 kHz (to heat up Fe_3O_4) + 30 mT at 0.25 Hz to actuate beam	100 (and above) in 40 s		dual magnetic field activation; elastic modulus increases linearly with ς; R_F = 95%; R_R = 100%	141
PLA	Fe_3O_4	10−40 wt %		magnetic	30 kA/m at 268 kHz	>60	>200	nonmonotonic evolution of R_R, modulus, tensile strength, and elongation at break with ς	132
Nafion	Fe_3O_4	15−25%		magnetic	Power 50−100%	internal T 50−110, surface T < 40	16	surface modification of Fe_3O_4 to improve distribution	219
PCL/PU	GNP	0−10 wt %	∼1 Ω m for 10 wt %	electrical	10−40 V	60 for 10 wt % at 10 V; 100 for 10 wt % at 30 V	60	Secovery within 1 min for 7 wt % at 30 V; faster heating and recovery for higher ς; T_g, χ_c, viscosity increase with ς; $T_m$and T_c decrease with ς	220
PLA	PPy		0.028 Ω m	electrical	15−40 V	120 for 40 V	2	microfiber membrane PPy coated; worse mechanical properties with Ppy ρ_e depends on polymerization time and temperature	221
PCLA	GO	4.86−13.29 vol %		electrical			2.5	R_R = 100%	222
PU/EP	G and CNT	0.8−3 wt % CNT and 2−12 wt % graphene	0.31 Ω m for 12 wt % graphene	electrical	100 V for 8% graphene and 3% CNT	60	150	compressive strain; densification at ε > 70%; 2% permanent deformation after 100 cycles	223

intermediate shapes could widen the application of these materials.

(iii) Due to the specific requirements of the biomedical industry, surely more investigations will follow on biocompatible SMPs and SMCs that can be remotely actuated. Besides, if they are also biodegradable, some implants would not need a secondary surgical intervention to be removed.

https://doi.org/10.1021/acsomega.2c05930
ACS Omega XXXX, XXX, XXX−XXX

(iv) On the same green trend as biodegradability, dynamic covalent bonds on the SMP matrices will surely be kept under investigation. These allow for recyclability and reprocessability of the material. Similarly, research on self-healable SMCs is on the rise so as to increase the lifetime of the structures.

(v) Especially within the area of electrically activated SMCs, there has been recent interest in selectively and sequentially triggering the shape recovery. By improving the localization of heat generation, sequential shape recovery may lead to more applications of electroactive SMCs in self-deployable and self-foldable devices.

(vi) There are some cases where direct heating cannot be applied in order to trigger the shape recovery, such as when the material is surrounded by sensitive equipment or when it is inside of the human body. In general, the current trend in the investigation of SMCs is in multistimuli materials where, besides a conventional thermal treatment, alternative heating can be applied in order to trigger the shape memory effects remotely. These mechanisms include resistive heating, electromagnetic induction, and photothermal effects. An in-depth understanding of the energy conversion into heat of these alternative heating mechanisms may allow for complex and accurately actuated devices.

(vii) Because of the direct link between the material and the mechanical and shape memory properties of SMCs, a predictable and controllable temperature through alternative heating mechanisms (resistive Joule heating, electromagnetic induction, etc.) is desired.

(viii) Due to the one-time actuation or the required time-consuming shape reprogramming of conventional 1W-SM polymers and composites, materials exhibiting 2W-SM effects will likely be the object of future investigations in order to meet the challenging needs of future applications. Undoubtedly, more research is needed in this area to evaluate the fatigue and wearing of the 2W-SM characteristics in order to estimate the lifetime expectancy of these materials when in use. Similarly, the cyclic (or subcyclic) lifetime of multiple shape memory composites should be further investigated.

The outstanding and polyvalent characteristics of these materials offer an incredible platform to investigate and create applications that are, as of now, unimaginable.

APPENDIX

This appendix provides Table 1, giving some of the many references available in the literature of shape memory composites with certain fillers that allows them to be activated with either an electric field or a magnetic field. Some other characteristics of the materials or the experiments are given as additional information. For a better understanding of the information listed in the table, please refer to the list of abbreviations given below.

AUTHOR INFORMATION

Corresponding Authors

Clara Pereira Sánchez − *Department of Electrical Engineering and Computer Science, University of Liège, Liège 4000, Belgium*; Email: capereira@uliege.be

Christine Jérôme − *CERM, CESAM-RU, University of Liège, Liège 4000, Belgium*; orcid.org/0000-0001-8442-5740; Email: C.Jerome@uliege.be

Ludovic Noels − *Department of Aerospace and Mechanical Engineering, University of Liège, Liège 4000, Belgium*; Email: L.Noels@uliege.be

Philippe Vanderbemden − *Department of Electrical Engineering and Computer Science, University of Liège, Liège 4000, Belgium*; orcid.org/0000-0002-1436-7116; Email: philippe.vanderbemden@uliege.be

Complete contact information is available at: https://pubs.acs.org/10.1021/acsomega.2c05930

Notes

The authors declare no competing financial interest.

ACKNOWLEDGMENTS

This research was founded through the "Actions de recherche concertées 2017 − Synthesis, Characterization, and Multiscale Model of Smart Composite Materials (S3CM3) 17/21-07", financed by the "Direction Générale de l'Enseignement non obligatoire de la Recherche scientifique, Direction de la Recherche scientifique, Communauté française de Belgique et octroyées par l'Académie Universitaire Wallonie-Europe".

ABBREVIATIONS

BMI	bismaleimide
BR	butadiene rubber
C_p	heat capacity
CB	carbon black
CE	cyanate ester
CF	carbon fiber
CNF	carbon nanofiber
CNT	carbon nanotube
CSF	carbon short fiber
DMA	dimethacrylate
EOC	ethylene-1-octene copolymer
EP	epoxy
G	graphene
Gr	graphite
GO	graphene oxide
GNP	graphene nanoplatelets
LLDPE	linear low-density polyethylene
MA	methacrylate
MWCNT	multiwalled carbon nanotube
NGDE	neopentyl glycol diglycidyl ether
phr	parts per hundred rubber
PBS	poly(butylene succinate)
PCL	polycaprolactone
PCLA	poly(L-lactide-co-ε-caprolactone)
PCO	polycyclooctene
PDL	ω-pentadecalactone
PE	polyethylene
PEG	poly(ethylene glycol)
PEN	polyethylene naphthalate
PEVA	poly(ethylene-vinyl acetate)
PK	polyketone
PMMA	poly(methyl methacrylate)
PLA	poly(lactic acid)
PPC	poly(propylene carbonate)
PPDO	polydioxanone
PPy	polypyrrole

https://doi.org/10.1021/acsomega.2c05930
ACS Omega XXXX, XXX, XXX−XXX

PS	polystyrene
PU	polyurethane
PVA	polyvinyl acetate
PVAl	poly(vinyl alcohol)
PVDF	polyvinylidene fluoride
Py	pyrene
R_F	shape fixity ratio
rGO	reduced graphene oxide
R_R	shape recovery ratio
SBS	poly(styrene-butadiene-styrene)
SMA	shape memory alloy
SMP	shape memory polymer
T	temperature
T_c	crystallization temperature
T_g	glass transition temperature
T_m	melting temperature
t_R	recovery time
ε	strain
κ	thermal conductivity
ρ_e	electrical resistivity
ς	concentration
χ_c	crystallinity
2W-SM	two-way shape memory

REFERENCES

(1) Parameswaranpillai, J.; Siengchin, S.; George, J. J.; Jose, S. *Shape Memory Polymers, Blends and Composites: Advances and Applications; Advanced Structured Materials*; Springer Singapore: 2020; Vol. *115*. DOI: 10.1007/978-981-13-8574-2.

(2) Behl, M.; Lendlein, A. Actively Moving Polymers. *Soft Matter* **2007**, *3* (1), 58−67.

(3) Xin, X.; Liu, L.; Liu, Y.; Leng, J. Mechanical Models, Structures, and Applications of Shape-Memory Polymers and Their Composites. *Acta Mech. Solida Sin.* **2019**, *32* (5), 535−565.

(4) Lendlein, A.; Behl, M.; Hiebl, B.; Wischke, C. Shape-Memory Polymers as a Technology Platform for Biomedical Applications. *Expert Rev. Med. Devices* **2010**, *7* (3), 357−379.

(5) Mazurek-Budzyńska, M.; Razzaq, M. Y.; Behl, M.; Lendlein, A. Shape-Memory Polymers. In *Functional Polymers*; Jafar Mazumder, M. A., Sheardown, H., Al-Ahmed, A., Eds.; Springer International: 2019; Polymers and Polymeric Composites: A Reference Series, pp 605−663. DOI: 10.1007/978-3-319-95987-0_18.

(6) Liu, C.; Qin, H.; Mather, P. T. Review of Progress in Shape-Memory Polymers. *J. Mater. Chem.* **2007**, *17* (16), 1543.

(7) Rousseau, I. A. Challenges of Shape Memory Polymers: A Review of the Progress toward Overcoming SMP's Limitations. *Polym. Eng. Sci.* **2008**, *48* (11), 2075−2089.

(8) Leng, J.; Lu, H.; Liu, Y.; Huang, W. M.; Du, S. Shape-Memory Polymers—A Class of Novel Smart Materials. *MRS Bull.* **2009**, *34* (11), 848−855.

(9) Hu, J. Introduction to Shape Memory Polymers. In *Advances in Shape Memory Polymers*; Elsevier: 2013; pp 1−22. DOI: 10.1533/9780857098542.1.

(10) Safranski, D. L. Introduction to Shape-Memory Polymers. In *Shape-Memory Polymer Device Design*; Elsevier: 2017; pp 1−22. DOI: 10.1016/B978-0-323-37797-3.00001-4.

(11) Yakacki, C. M.; Shandas, R.; Safranski, D.; Ortega, A. M.; Sassaman, K.; Gall, K. Strong, Tailored, Biocompatible Shape-Memory Polymer Networks. *Adv. Funct. Mater.* **2008**, *18* (16), 2428−2435.

(12) Hu, J. *Shape Memory Polymers: Fundamentals, Advances and Applications*; Smithers: 2014.

(13) Hager, M. D.; Bode, S.; Weber, C.; Schubert, U. S. Shape Memory Polymers: Past, Present and Future Developments. *Prog. Polym. Sci.* **2015**, *49* (50), 3−33.

(14) Huang, S.; Kong, X.; Xiong, Y.; Zhang, X.; Chen, H.; Jiang, W.; Niu, Y.; Xu, W.; Ren, C. An Overview of Dynamic Covalent Bonds in Polymer Material and Their Applications. *Eur. Polym. J.* **2020**, *141*, 110094.

(15) García, F.; Smulders, M. M. J. Dynamic Covalent Polymers. *J. Polym. Sci., Part A: Polym. Chem.* **2016**, *54* (22), 3551−3577.

(16) Hammer, L.; Van Zee, N. J.; Nicolaÿ, R. Dually Crosslinked Polymer Networks Incorporating Dynamic Covalent Bonds. *Polymers* **2021**, *13* (3), 396.

(17) Li, Z.; Yu, R.; Guo, B. Shape-Memory and Self-Healing Polymers Based on Dynamic Covalent Bonds and Dynamic Noncovalent Interactions: Synthesis, Mechanism, and Application. *ACS Appl. Bio Mater.* **2021**, *4* (8), 5926−5943.

(18) Peng, S.; Sun, Y.; Ma, C.; Duan, G.; Liu, Z.; Ma, C. Recent Advances in Dynamic Covalent Bond-Based Shape Memory Polymers. *e-Polym.* **2022**, *22* (1), 285−300.

(19) Koltzenburg, S.; Maskos, M.; Nuyken, O. Elastomers. In *Polymer Chemistry*; Springer Berlin Heidelberg: 2017; pp 477−491. DOI: 10.1007/978-3-662-49279-6_18.

(20) Tobushi, H.; Hara, H.; Yamada, E.; Hayashi, S. Thermomechanical Properties in a Thin Film of Shape Memory Polymer of Polyurethane Series. *Smart Mater. Struct.* **1996**, *5* (4), 483−491.

(21) Lendlein, A.; Langer, R. Biodegradable, Elastic Shape-Memory Polymers for Potential Biomedical Applications. *Science* **2002**, *296* (5573), 1673−1676.

(22) Miaudet, P.; Derré, A.; Maugey, M.; Zakri, C.; Piccione, P. M.; Inoubli, R.; Poulin, P. Shape and Temperature Memory of Nanocomposites with Broadened Glass Transition. *Science* **2007**, *318* (5854), 1294−1296.

(23) Ni, Q.-Q.; Zhang, C.; Fu, Y.; Dai, G.; Kimura, T. Shape Memory Effect and Mechanical Properties of Carbon Nanotube/Shape Memory Polymer Nanocomposites. *Compos. Struct.* **2007**, *81* (2), 176−184.

(24) Behl, M.; Zotzmann, J.; Lendlein, A. One-Way and Reversible Dual-Shape Effect of Polymer Networks Based on Polypentadecalactone Segments. *Int. J. Artif Organs* **2011**, *34* (2), 231−237.

(25) Gopinath, S.; Adarsh, N. N.; Radhakrishnan Nair, P.; Mathew, S. One-Way Thermo-Responsive Shape Memory Polymer Nanocomposite Derived from Polycaprolactone and Polystyrene-Block-Polybutadiene-Block-Polystyrene Packed with Carbon Nanofiber. *Mater. Today Commun.* **2020**, *22*, 100802.

(26) Leng, J.; Lan, X.; Liu, Y.; Du, S. Shape-Memory Polymers and Their Composites: Stimulus Methods and Applications. *Prog. Mater. Sci.* **2011**, *56* (7), 1077−1135.

(27) Bothe, M. *Shape Memory and Actuation Behavior of Semicrystalline Polymer Networks*; BAM-Dissertationsreihe; BAM: 2014.

(28) Zare, M.; Prabhakaran, M. P.; Parvin, N.; Ramakrishna, S. Thermally-Induced Two-Way Shape Memory Polymers: Mechanisms, Structures, and Applications. *Chem. Eng. J.* **2019**, *374*, 706−720.

(29) Chung, T.; Romo-Uribe, A.; Mather, P. T. Two-Way Reversible Shape Memory in a Semicrystalline Network. *Macromolecules* **2008**, *41* (1), 184−192.

(30) Murcia, A. P.; Gomez, J. M. U.; Sommer, J.-U.; Ionov, L. Two-Way Shape Memory Polymers: Evolution of Stress *vs* Evolution of Elongation. *Macromolecules* **2021**, *54* (12), 5838−5847.

(31) Pilate, F.; Toncheva, A.; Dubois, P.; Raquez, J.-M. Shape-Memory Polymers for Multiple Applications in the Materials World. *Eur. Polym. J.* **2016**, *80*, 268−294.

(32) Hong, S. J.; Yu, W.-R.; Youk, J. H. Two-Way Shape Memory Behavior of Shape Memory Polyurethanes with a Bias Load. *Smart Mater. Struct.* **2010**, *19* (3), 035022.

(33) Westbrook, K. K.; Parakh, V.; Chung, T.; Mather, P. T.; Wan, L. C.; Dunn, M. L.; Qi, H. J. Constitutive Modeling of Shape Memory Effects in Semicrystalline Polymers With Stretch Induced Crystallization. *J. Eng. Mater. Technol.* **2010**, *132* (4), 041010.

(34) Li, J.; Rodgers, W. R.; Xie, T. Semi-Crystalline Two-Way Shape Memory Elastomer. *Polymer* **2011**, *52* (23), 5320−5325.

(35) Pandini, S.; Passera, S.; Messori, M.; Paderni, K.; Toselli, M.; Gianoncelli, A.; Bontempi, E.; Riccò, T. Two-Way Reversible Shape Memory Behaviour of Crosslinked Poly(ε-Caprolactone). *Polymer* **2012**, *53* (9), 1915−1924.

https://doi.org/10.1021/acsomega.2c05930
ACS Omega XXXX, XXX, XXX−XXX

(36) Ge, Q.; Westbrook, K. K.; Mather, P. T.; Dunn, M. L.; Jerry Qi, H. Thermomechanical Behavior of a Two-Way Shape Memory Composite Actuator. *Smart Mater. Struct.* **2013**, *22* (5), 055009.
(37) Huang, M.; Dong, X.; Wang, L.; Zhao, J.; Liu, G.; Wang, D. Two-Way Shape Memory Property and Its Structural Origin of Cross-Linked Poly(ε-Caprolactone). *RSC Adv.* **2014**, *4* (98), 55483−55494.
(38) Kolesov, I.; Dolynchuk, O.; Jehnichen, D.; Reuter, U.; Stamm, M.; Radusch, H.-J. Changes of Crystal Structure and Morphology during Two-Way Shape-Memory Cycles in Cross-Linked Linear and Short-Chain Branched Polyethylenes. *Macromolecules* **2015**, *48* (13), 4438−4450.
(39) Ma, L.; Zhao, J.; Wang, X.; Chen, M.; Liang, Y.; Wang, Z.; Yu, Z.; Hedden, R. C. Effects of Carbon Black Nanoparticles on Two-Way Reversible Shape Memory in Crosslinked Polyethylene. *Polymer* **2015**, *56*, 490−497.
(40) Yang, Q.; Fan, J.; Li, G. Artificial Muscles Made of Chiral Two-Way Shape Memory Polymer Fibers. *Appl. Phys. Lett.* **2016**, *109* (18), 183701.
(41) Xie, H.; Cheng, C.-Y.; Deng, X.-Y.; Fan, C.-J.; Du, L.; Yang, K.-K.; Wang, Y.-Z. Creating Poly(Tetramethylene Oxide) Glycol-Based Networks with Tunable Two-Way Shape Memory Effects via Temperature-Switched Netpoints. *Macromolecules* **2017**, *50* (13), 5155−5164.
(42) Hui, J.; Xia, H.; Chen, H.; Qiu, Y.; Fu, Y.; Ni, Q.-Q. Two-Way Reversible Shape Memory Polymer: Synthesis and Characterization of Benzoyl Peroxide-Crosslinked Poly(Ethylene-Co-Vinyl Acetate). *Mater. Lett.* **2020**, *258*, 126762.
(43) Raquez, J.-M.; Vanderstappen, S.; Meyer, F.; Verge, P.; Alexandre, M.; Thomassin, J.-M.; Jérôme, C.; Dubois, P. Design of Cross-Linked Semicrystalline Poly(ε-Caprolactone)-Based Networks with One-Way and Two-Way Shape-Memory Properties through Diels-Alder Reactions. *Chem. - Eur. J.* **2011**, *17* (36), 10135−10143.
(44) Behl, M.; Kratz, K.; Zotzmann, J.; Nöchel, U.; Lendlein, A. Reversible Bidirectional Shape-Memory Polymers. *Adv. Mater.* **2013**, *25* (32), 4466−4469.
(45) Bothe, M.; Pretsch, T. Bidirectional Actuation of a Thermoplastic Polyurethane Elastomer. *J. Mater. Chem. A* **2013**, *1* (46), 14491.
(46) Biswas, A.; Aswal, V. K.; Sastry, P. U.; Rana, D.; Maiti, P. Reversible Bidirectional Shape Memory Effect in Polyurethanes through Molecular Flipping. *Macromolecules* **2016**, *49* (13), 4889−4897.
(47) Wang, K.; Jia, Y.-G.; Zhu, X. X. Two-Way Reversible Shape Memory Polymers Made of Cross-Linked Cocrystallizable Random Copolymers with Tunable Actuation Temperatures. *Macromolecules* **2017**, *50* (21), 8570−8579.
(48) Xu, Z.; Ding, C.; Wei, D.-W.; Bao, R.-Y.; Ke, K.; Liu, Z.; Yang, M.-B.; Yang, W. Electro and Light-Active Actuators Based on Reversible Shape-Memory Polymer Composites with Segregated Conductive Networks. *ACS Appl. Mater. Interfaces* **2019**, *11* (33), 30332−30340.
(49) Burke, K. A.; Mather, P. T. Soft Shape Memory in Main-Chain Liquid Crystalline Elastomers. *J. Mater. Chem.* **2010**, *20* (17), 3449.
(50) Wang, Y.; Huang, X.; Zhang, J.; Bi, M.; Zhang, J.; Niu, H.; Li, C.; Yu, H.; Wang, B.; Jiang, H. Two-Step Crosslinked Liquid-Crystalline Elastomer with Reversible Two-Way Shape Memory Characteristics. *Mol. Cryst. Liq. Cryst.* **2017**, *650* (1), 13−22.
(51) Chen, S.; Hu, J.; Zhuo, H.; Zhu, Y. Two-Way Shape Memory Effect in Polymer Laminates. *Mater. Lett.* **2008**, *62* (25), 4088−4090.
(52) Tobushi, H.; Hayashi, S.; Sugimoto, Y.; Date, K. Two-Way Bending Properties of Shape Memory Composite with SMA and SMP. *Materials* **2009**, *2* (3), 1180−1192.
(53) Wang, K.; Jia, Y.-G.; Zhao, C.; Zhu, X. X. Multiple and Two-Way Reversible Shape Memory Polymers: Design Strategies and Applications. *Prog. Mater. Sci.* **2019**, *105*, 100572.
(54) Xia, Y.; He, Y.; Zhang, F.; Liu, Y.; Leng, J. A Review of Shape Memory Polymers and Composites: Mechanisms, Materials, and Applications. *Adv. Mater.* **2021**, *33* (6), 2000713.
(55) Dolog, R.; Weiss, R. A. Shape Memory Behavior of a Polyethylene-Based Carboxylate Ionomer. *Macromolecules* **2013**, *46* (19), 7845−7852.
(56) Wang, K.; Jia, Y.-G.; Zhu, X. X. Biocompound-Based Multiple Shape Memory Polymers Reinforced by Photo-Cross-Linking. *ACS Biomater. Sci. Eng.* **2015**, *1* (9), 855−863.
(57) Dai, L.; Song, J.; Qu, S.; Xiao, R. Triple-Shape Memory Effect in 3D-Printed Polymers. *Express Polym. Lett.* **2020**, *14* (12), 1116−1126.
(58) Pretsch, T. Triple-Shape Properties of a Thermoresponsive Poly(Ester Urethane). *Smart Mater. Struct.* **2010**, *19* (1), 015006.
(59) Zotzmann, J.; Behl, M.; Feng, Y.; Lendlein, A. Copolymer Networks Based on Poly(ω-Pentadecalactone) and Poly(ε-Caprolactone)Segments as a Versatile Triple-Shape Polymer System. *Adv. Funct. Mater.* **2010**, *20* (20), 3583−3594.
(60) Chatani, S.; Wang, C.; Podgórski, M.; Bowman, C. N. Triple Shape Memory Materials Incorporating Two Distinct Polymer Networks Formed by Selective Thiol−Michael Addition Reactions. *Macromolecules* **2014**, *47* (15), 4949−4954.
(61) Xie, T.; Xiao, X.; Cheng, Y.-T. Revealing Triple-Shape Memory Effect by Polymer Bilayers: Revealing Triple-Shape Memory Effect by Polymer Bilayers. *Macromol. Rapid Commun.* **2009**, *30* (21), 1823−1827.
(62) Tobushi, H.; Hayashi, S.; Pieczyska, E.; Date, K.; Nishimura, Y. Three-Way Shape Memory Composite Actuator. *MSF* **2011**, *674*, 225−230.
(63) Scalet, G. Two-Way and Multiple-Way Shape Memory Polymers for Soft Robotics: An Overview. *Actuators* **2020**, *9* (1), 10.
(64) Huang, Y. N.; Fan, L. F.; Rong, M. Z.; Zhang, M. Q.; Gao, Y. M. External Stress-Free Reversible Multiple Shape Memory Polymers. *ACS Appl. Mater. Interfaces* **2019**, *11* (34), 31346−31355.
(65) Li, J.; Liu, T.; Xia, S.; Pan, Y.; Zheng, Z.; Ding, X.; Peng, Y. A Versatile Approach to Achieve Quintuple-Shape Memory Effect by Semi-Interpenetrating Polymer Networks Containing Broadened Glass Transition and Crystalline Segments. *J. Mater. Chem.* **2011**, *21* (33), 12213.
(66) Shao, Y.; Lavigueur, C.; Zhu, X. X. Multishape Memory Effect of Norbornene-Based Copolymers with Cholic Acid Pendant Groups. *Macromolecules* **2012**, *45* (4), 1924−1930.
(67) Kong, D.; Xiao, X. High Cycle-Life Shape Memory Polymer at High Temperature. *Sci. Rep* **2016**, *6* (1), 33610.
(68) Rodinò, S.; Curcio, E. M.; Renzo, D. A.; Sgambitterra, E.; Magarò, P.; Furgiuele, F.; Brandizzi, M.; Maletta, C. Shape Memory Alloy—Polymer Composites: Static and Fatigue Pullout Strength under Thermo-Mechanical Loading. *Materials* **2022**, *15* (9), 3216.
(69) Lu, L.; Li, G. One-Way Multishape-Memory Effect and Tunable Two-Way Shape Memory Effect of Ionomer Poly(Ethylene- *Co* -Methacrylic Acid). *ACS Appl. Mater. Interfaces* **2016**, *8* (23), 14812−14823.
(70) Cotin, G.; Perton, F.; Blanco-Andujar, C.; Pichon, B.; Mertz, D.; Bégin-Colin, S. Design of Anisotropic Iron-Oxide-Based Nanoparticles for Magnetic Hyperthermia. In *Nanomaterials for Magnetic and Optical Hyperthermia Applications*; Elsevier: 2019; pp 41−60. DOI: 10.1016/B978-0-12-813928-8.00002-8.
(71) Li, Q.; Kartikowati, C. W.; Horie, S.; Ogi, T.; Iwaki, T.; Okuyama, K. Correlation between Particle Size/Domain Structure and Magnetic Properties of Highly Crystalline Fe3O4 Nanoparticles. *Sci. Rep* **2017**, *7* (1), 9894.
(72) Yani, A.; Kurniawan, C.; Djuhana, D. *Investigation of the Ground State Domain Structure Transition on Magnetite (Fe3O4)*; Bali: 2018; p 020020. DOI: 10.1063/1.5064017.
(73) Soto, G. D.; Meiorin, C.; Actis, D. G.; Mendoza Zélis, P.; Moscoso Londoño, O.; Muraca, D.; Mosiewicki, M. A.; Marcovich, N. E. Magnetic Nanocomposites Based on Shape Memory Polyurethanes. *Eur. Polym. J.* **2018**, *109*, 8−15.
(74) Meng, Q.; Hu, J. A Review of Shape Memory Polymer Composites and Blends. *Composites, Part A* **2009**, *40* (11), 1661−1672.
(75) Cheng, X.; Chen, Y.; Dai, S.; Bilek, M. M. M.; Bao, S.; Ye, L. Bending Shape Memory Behaviours of Carbon Fibre Reinforced Polyurethane-Type Shape Memory Polymer Composites under Relatively Small Deformation: Characterisation and Computational Simulation. *J. Mech. Behav. Biomed. Mater.* **2019**, *100*, 103372.

https://doi.org/10.1021/acsomega.2c05930
ACS Omega XXXX, XXX, XXX−XXX

(76) Cuevas, J. M.; Rubio, R.; Laza, J. M.; Vilas, J. L.; Rodriguez, M.; M León, L. Shape Memory Composites Based on Glass-Fibre-Reinforced Poly(Ethylene)-like Polymers. *Smart Mater. Struct.* **2012**, *21* (3), 035004.
(77) Korotkov, R.; Vedernikov, A.; Gusev, S.; Alajarmeh, O.; Akhatov, I.; Safonov, A. Shape Memory Behavior of Unidirectional Pultruded Laminate. *Composites, Part A* **2021**, *150*, 106609.
(78) Guo, J.; Lv, H.; Wang, Z.; Tang, X.; Liang, W.; Zhang, S. Thermo-Mechanical Property of Shape Memory Polymer/Carbon Fibre Composites. *Mater. Res. Innovations* **2015**, *19* (sup8), S8-566−S8-572.
(79) Wang, Z.; Liu, J.; Guo, J.; Sun, X.; Xu, L. The Study of Thermal, Mechanical and Shape Memory Properties of Chopped Carbon Fiber-Reinforced TPI Shape Memory Polymer Composites. *Polymers* **2017**, *9* (11), 594.
(80) Pulla, S. S. *Development of Multifunctional Shape Memory Polymer and Shape Memory Polymer Composites*; University of Kentucky: 2015.
(81) Wang, Y.; Chen, Z.; Niu, J.; Shi, Y.; Zhao, J.; Ye, J.; Tian, W. Electrically Responsive Shape Memory Composites Using Silver Plated Chopped Carbon Fiber. *Front. Chem.* **2020**, *8*, 322.
(82) Qi, Y.; Sun, B.; Gu, B.; Zhang, W. Electrothermally Actuated Properties of Fabric-Reinforced Shape Memory Polymer Composites Based on Core−Shell Yarn. *Compos. Struct.* **2022**, *292*, 115681.
(83) Margoy, D.; Gouzman, I.; Grossman, E.; Bolker, A.; Eliaz, N.; Verker, R. Epoxy-Based Shape Memory Composite for Space Applications. *Acta Astronautica* **2021**, *178*, 908−919.
(84) Meng, H.; Li, G. A Review of Stimuli-Responsive Shape Memory Polymer Composites. *Polymer* **2013**, *54* (9), 2199−2221.
(85) Le, H. H.; Osazuwa, O.; Kolesov, I.; Ilisch, S.; Radusch, H.-J. Influence of Carbon Black Properties on the Joule Heating Stimulated Shape-Memory Behavior of Filledethylene-1-Octene Copolymer. *Polym. Eng. Sci.* **2011**, *51* (3), 500−508.
(86) Arun, D. I.; Santhosh Kumar, K. S.; Satheesh Kumar, B.; Chakravarthy, P.; Dona, M.; Santhosh, B. High Glass-Transition Polyurethane-Carbon Black Electro-Active Shape Memory Nanocomposite for Aerospace Systems. *Mater. Sci. Technol.* **2019**, *35* (5), 596−605.
(87) González-Jiménez, A.; Bernal-Ortega, P.; Salamanca, F. M.; Valentin, J. L. Shape-Memory Composites Based on Ionic Elastomers. *Polymers* **2022**, *14* (6), 1230.
(88) Wang, X.; Zhao, J.; Chen, M.; Ma, L.; Zhao, X.; Dang, Z.-M.; Wang, Z. Improved Self-Healing of Polyethylene/Carbon Black Nanocomposites by Their Shape Memory Effect. *J. Phys. Chem. B* **2013**, *117* (5), 1467−1474.
(89) Gunes, I. S.; Jimenez, G. A.; Jana, S. C. Carbonaceous Fillers for Shape Memory Actuation of Polyurethane Composites by Resistive Heating. *Carbon* **2009**, *47* (4), 981−997.
(90) Tekay, E. Preparation and Characterization of Electro-Active Shape Memory PCL/SEBS-g-MA/MWCNT Nanocomposites. *Polymer* **2020**, *209*, 122989.
(91) Pötschke, P.; Villmow, T.; Krause, B. Melt Mixed PCL/MWCNT Composites Prepared at Different Rotation Speeds: Characterization of Rheological, Thermal, and Electrical Properties, Molecular Weight, MWCNT Macrodispersion, and MWCNT Length Distribution. *Polymer* **2013**, *54* (12), 3071−3078.
(92) Jung, Y. C.; Yoo, H. J.; Kim, Y. A.; Cho, J. W.; Endo, M. Electroactive Shape Memory Performance of Polyurethane Composite Having Homogeneously Dispersed and Covalently Crosslinked Carbon Nanotubes. *Carbon* **2010**, *48* (5), 1598−1603.
(93) Jin Yoo, H.; Chae Jung, Y.; Gopal Sahoo, N.; Whan Cho, J. Polyurethane-Carbon Nanotube Nanocomposites Prepared by In-Situ Polymerization with Electroactive Shape Memory. *J. Macromol. Sci., Part B: Phys.* **2006**, *45* (4), 441−451.
(94) Raja, M.; Ryu, S. H.; Shanmugharaj, A. M. Influence of Surface Modified Multiwalled Carbon Nanotubes on the Mechanical and Electroactive Shape Memory Properties of Polyurethane (PU)/Poly(Vinylidene Diflouride) (PVDF) Composites. *Colloids Surf., A* **2014**, *450*, 59−66.
(95) Lu, H.; Gou, J. Fabrication and Electroactive Responsive Behavior of Shape-Memory Nanocomposite Incorporated with Self-Assembled Multiwalled Carbon Nanotube Nanopaper: Shape-Memory Nanocomposite. *Polym. Adv. Technol.* **2012**, *23* (12), 1529−1535.
(96) Lu, H.; Liu, Y.; Gou, J.; Leng, J.; Du, S. Surface Coating of Multi-Walled Carbon Nanotube Nanopaper on Shape-Memory Polymer for Multifunctionalization. *Compos. Sci. Technol.* **2011**, *71* (11), 1427−1434.
(97) Slobodian, P.; Riha, P.; Olejnik, R.; Matyas, J. Accelerated Shape Forming and Recovering, Induction, and Release of Adhesiveness of Conductive Carbon Nanotube/Epoxy Composites by Joule Heating. *Polymers* **2020**, *12* (5), 1030.
(98) Datta, S.; Henry, T. C.; Sliozberg, Y. R.; Lawrence, B. D.; Chattopadhyay, A.; Hall, A. J. Carbon Nanotube Enhanced Shape Memory Epoxy for Improved Mechanical Properties and Electroactive Shape Recovery. *Polymer* **2021**, *212*, 123158.
(99) Wang, X.; Sparkman, J.; Gou, J. Electrical Actuation and Shape Memory Behavior of Polyurethane Composites Incorporated with Printed Carbon Nanotube Layers. *Compos. Sci. Technol.* **2017**, *141*, 8−15.
(100) Pereira Sánchez, C.; Houbben, M.; Fagnard, J.-F.; Laurent, P.; Jérôme, C.; Noels, L.; Vanderbemden, P. Resistive Heating of a Shape Memory Composite: Analytical, Numerical and Experimental Study. *Smart Mater. Struct.* **2022**, *31* (2), 025003.
(101) Pereira Sánchez, C.; Houbben, M.; Fagnard, J.-F.; Harmeling, P.; Jérôme, C.; Noels, L.; Vanderbemden, P. Experimental Characterization of the Thermo-Electro-Mechanical Properties of a Shape Memory Composite during Electric Activation. *Smart Mater. Struct.* **2022**, *31* (9), 095029.
(102) Cortés, A.; Pérez-Chao, N.; Jiménez-Suárez, A.; Campo, M.; Prolongo, S. G. Sequential and Selective Shape Memory by Remote Electrical Control. *Eur. Polym. J.* **2022**, *164*, 110888.
(103) Cortés, A.; Aguilar, J. L.; Cosola, A.; Fernández Sanchez-Romate, X. X.; Jiménez-Suárez, A.; Sangermano, M.; Campo, M.; Prolongo, S. G. 4D-Printed Resins and Nanocomposites Thermally Stimulated by Conventional Heating and IR Radiation. *ACS Appl. Polym. Mater.* **2021**, *3* (10), 5207−5215.
(104) Xiao, W.-X.; Fan, C.-J.; Li, B.; Liu, W.-X.; Yang, K.-K.; Wang, Y.-Z. Single-Walled Carbon Nanotubes as Adaptable One-Dimensional Crosslinker to Bridge Multi-Responsive Shape Memory Network via $\pi-\pi$ Stacking. *Compos. Commun.* **2019**, *14*, 48−54.
(105) Park, C.; Wilkinson, J.; Banda, S.; Ounaies, Z.; Wise, K. E.; Sauti, G.; Lillehei, P. T.; Harrison, J. S. Aligned Single-Wall Carbon Nanotube Polymer Composites Using an Electric Field. *J. Polym. Sci. B Polym. Phys.* **2006**, *44* (12), 1751−1762.
(106) Martin, C. A.; Sandler, J. K. W.; Windle, A. H.; Schwarz, M.-K.; Bauhofer, W.; Schulte, K.; Shaffer, M. S. P. Electric Field-Induced Aligned Multi-Wall Carbon Nanotube Networks in Epoxy Composites. *Polymer* **2005**, *46* (3), 877−886.
(107) Yu, K.; Zhang, Z.; Liu, Y.; Leng, J. Carbon Nanotube Chains in a Shape Memory Polymer/Carbon Black Composite: To Significantly Reduce the Electrical Resistivity. *Appl. Phys. Lett.* **2011**, *98* (7), 074102.
(108) Sanchez-Garcia, M. D.; Lagaron, J. M.; Hoa, S. V. Effect of Addition of Carbon Nanofibers and Carbon Nanotubes on Properties of Thermoplastic Biopolymers. *Compos. Sci. Technol.* **2010**, *70* (7), 1095−1105.
(109) Gong, X.; Liu, L.; Liu, Y.; Leng, J. An Electrical-Heating and Self-Sensing Shape Memory Polymer Composite Incorporated with Carbon Fiber Felt. *Smart Mater. Struct.* **2016**, *25* (3), 035036.
(110) Wang, W.; Liu, D.; Liu, Y.; Leng, J.; Bhattacharyya, D. Electrical Actuation Properties of Reduced Graphene Oxide Paper/Epoxy-Based Shape Memory Composites. *Compos. Sci. Technol.* **2015**, *106*, 20−24.
(111) Jiu, H.; Jiao, H.; Zhang, L.; Zhang, S.; Zhao, Y. Graphene-Crosslinked Two-Way Reversible Shape Memory Polyurethane Nanocomposites with Enhanced Mechanical and Electrical Properties. *J. Mater. Sci: Mater. Electron* **2016**, *27* (10), 10720−10728.
(112) Martin-Gallego, M.; Verdejo, R.; Lopez-Manchado, M. A.; Sangermano, M. Epoxy-Graphene UV-Cured Nanocomposites. *Polymer* **2011**, *52* (21), 4664−4669.

https://doi.org/10.1021/acsomega.2c05930
ACS Omega XXXX, XXX, XXX−XXX

(113) Kim, J. T.; Kim, B. K.; Kim, E. Y.; Park, H. C.; Jeong, H. M. Synthesis and Shape Memory Performance of Polyurethane/Graphene Nanocomposites. *React. Funct. Polym.* **2014**, *74*, 16−21.
(114) Kim, J. T.; Jeong, H. J.; Park, H. C.; Jeong, H. M.; Bae, S. Y.; Kim, B. K. Electroactive Shape Memory Performance of Polyurethane/Graphene Nanocomposites. *React. Funct. Polym.* **2015**, *88*, 1−7.
(115) Sabzi, M.; Babaahmadi, M.; Samadi, N.; Mahdavinia, G. R.; Keramati, M.; Nikfarjam, N. Graphene Network Enabled High Speed Electrical Actuation of Shape Memory Nanocomposite Based on Poly(Vinyl Acetate): Shape Memory Nanocomposites of Poly(Vinyl Acetate). *Polym. Int.* **2017**, *66* (5), 665−671.
(116) Thinh, P. X.; Basavajara, C.; Kim, J. K.; Huh, D. S. Characterization and Electrical Properties of Honeycomb-Patterned Poly(ε-Caprolactone)/Reduced Graphene Oxide Composite Film. *Polym. Compos* **2012**, *33* (12), 2159−2168.
(117) Chen, Y.-F.; Tan, Y.-J.; Li, J.; Hao, Y.-B.; Shi, Y.-D.; Wang, M. Graphene Oxide-Assisted Dispersion of Multi-Walled Carbon Nanotubes in Biodegradable Poly(ε-Caprolactone) for Mechanical and Electrically Conductive Enhancement. *Polym. Test.* **2018**, *65*, 387−397.
(118) Kang, S.; Kang, T.-H.; Kim, B. S.; Oh, J.; Park, S.; Choi, I. S.; Lee, J.; Son, J. G. 2D Reentrant Micro-Honeycomb Structure of Graphene-CNT in Polyurethane: High Stretchability, Superior Electrical/Thermal Conductivity, and Improved Shape Memory Properties. *Composites, Part B* **2019**, *162*, 580−588.
(119) Su, X.; Wang, R.; Li, X.; Araby, S.; Kuan, H.-C.; Naeem, M.; Ma, J. A Comparative Study of Polymer Nanocomposites Containing Multi-Walled Carbon Nanotubes and Graphene Nanoplatelets. *Nano Mater. Sci.* **2022**, *4*, 185−204.
(120) Chen, L.; Li, W.; Liu, Y.; Leng, J. Nanocomposites of Epoxy-Based Shape Memory Polymer and Thermally Reduced Graphite Oxide: Mechanical, Thermal and Shape Memory Characterizations. *Composites, Part B* **2016**, *91*, 75−82.
(121) Zhang, Y.; Hu, J.; Zhu, S.; Qin, T.; Ji, F. A "Trampoline" Nanocomposite: Tuning the Interlayer Spacing in Graphene Oxide/Polyurethane to Achieve Coalesced Mechanical and Memory Properties. *Compos. Sci. Technol.* **2019**, *180*, 14−22.
(122) Kausar, A. Shape Memory Polymer/Graphene Nanocomposites: State-of-the-Art. *e-Polym.* **2022**, *22* (1), 165−181.
(123) van Vilsteren, S. J. M.; Yarmand, H.; Ghodrat, S. Review of Magnetic Shape Memory Polymers and Magnetic Soft Materials. *Magnetochemistry* **2021**, *7* (9), 123.
(124) Gopinath, S.; Adarsh, N. N.; Nair, P.; Mathew, S. Nano-metal Oxide Fillers in Thermo-responsive Polycaprolactone-based Polymer Nanocomposites Smart Materials: Impact on Thermo-mechanical, and Shape Memory Properties. *J. Vinyl Addit Technol.* **2021**, *27* (4), 768−780.
(125) Aaltio, I.; Nilsén, F.; Lehtonen, J.; Ge, Y. L.; Spoljaric, S.; Seppälä, J.; Hannula, S. P. Magnetic Shape Memory - Polymer Hybrids. *MSF* **2016**, *879*, 133−138.
(126) Zhang, D. W.; Liu, Y. J.; Leng, J. S. Magnetic Field Activation of Thermoresponsive Shape-Memory Polymer with Embedded Micron Sized Ni Powder. *AMR* **2010**, *123−125*, 995−998.
(127) Buckley, P. R.; McKinley, G. H.; Wilson, T. S.; Small, W.; Benett, W. J.; Bearinger, J. P.; McElfresh, M. W.; Maitland, D. J. Inductively Heated Shape Memory Polymer for the Magnetic Actuation of Medical Devices. *IEEE Trans. Biomed. Eng.* **2006**, *53* (10), 2075−2083.
(128) Bayerl, T. *Application of Particulate Susceptors for the Inductive Heating of Temperature Sensitive Polymer-Polymer Composites, Als Ms. gedr.; IVW-Schriftenreihe*; Univ. Inst. für Verbundwerkstoffe: 2012.
(129) Deatsch, A. E.; Evans, B. A. Heating Efficiency in Magnetic Nanoparticle Hyperthermia. *J. Magn. Magn. Mater.* **2014**, *354*, 163−172.
(130) Magaye, R.; Zhao, J.; Bowman, L.; Ding, M. Genotoxicity and Carcinogenicity of Cobalt-, Nickel- and Copper-Based Nanoparticles. *Exp. Ther. Med.* **2012**, *4* (4), 551−561.
(131) Suwanwatana, W.; Yarlagadda, S.; Gillespie, J. W. Influence of Particle Size on Hysteresis Heating Behavior of Nickel Particulate Polymer Films. *Compos. Sci. Technol.* **2006**, *66* (15), 2825−2836.
(132) Zhang, X.; Lu, X.; Wang, Z.; Wang, J.; Sun, Z. Biodegradable Shape Memory Nanocomposites with Thermal and Magnetic Field Responsiveness. *J. Biomater. Sci., Polym. Ed.* **2013**, *24* (9), 1057−1070.
(133) Puig, J.; Hoppe, C. E.; Fasce, L. A.; Pérez, C. J.; Piñeiro-Redondo, Y.; Bañobre-López, M.; López-Quintela, M. A.; Rivas, J.; Williams, R. J. J. Superparamagnetic Nanocomposites Based on the Dispersion of Oleic Acid-Stabilized Magnetite Nanoparticles in a Diglycidylether of Bisphenol A-Based Epoxy Matrix: Magnetic Hyperthermia and Shape Memory. *J. Phys. Chem. C* **2012**, *116* (24), 13421−13428.
(134) Shahdan, D.; Flaifel, M. H.; Ahmad, S. H.; Chen, R. S.; Razak, J. A. Enhanced Magnetic Nanoparticles Dispersion Effect on the Behaviour of Ultrasonication-Assisted Compounding Processing of PLA/LNR/NiZn Nanocomposites. *Journal of Materials Research and Technology* **2021**, *15*, 5988−6000.
(135) Mohr, R.; Kratz, K.; Weigel, T.; Lucka-Gabor, M.; Moneke, M.; Lendlein, A. Initiation of Shape-Memory Effect by Inductive Heating of Magnetic Nanoparticles in Thermoplastic Polymers. *Proc. Natl. Acad. Sci. U.S.A.* **2006**, *103* (10), 3540−3545.
(136) Weigel, T.; Mohr, R.; Lendlein, A. Investigation of Parameters to Achieve Temperatures Required to Initiate the Shape-Memory Effect of Magnetic Nanocomposites by Inductive Heating. *Smart Mater. Struct.* **2009**, *18* (2), 025011.
(137) He, Z.; Satarkar, N.; Xie, T.; Cheng, Y.-T.; Hilt, J. Z. Remote Controlled Multishape Polymer Nanocomposites with Selective Radiofrequency Actuations. *Adv. Mater.* **2011**, *23* (28), 3192−3196.
(138) Lipert, K.; Ritschel, M.; Leonhardt, A.; Krupskaya, Y.; Büchner, B.; Klingeler, R. Magnetic Properties of Carbon Nanotubes with and without Catalyst. *J. Phys.: Conf. Ser.* **2010**, *200* (7), 072061.
(139) Kletetschka, G.; Inoue, Y.; Lindauer, J.; Hůlka, Z. Magnetic Tunneling with CNT-Based Metamaterial. *Sci. Rep* **2019**, *9* (1), 2551.
(140) Han, M.; Deng, L. High Frequency Properties of Carbon Nanotubes and Their Electromagnetic Wave Absorption Properties. In *Carbon Nanotubes Applications on Electron Devices*; Marulanda, J. M., Ed.; InTech: 2011. DOI: 10.5772/16629.
(141) Ze, Q.; Kuang, X.; Wu, S.; Wong, J.; Montgomery, S. M.; Zhang, R.; Kovitz, J. M.; Yang, F.; Qi, H. J.; Zhao, R. Magnetic Shape Memory Polymers with Integrated Multifunctional Shape Manipulation. *Adv. Mater.* **2020**, *32* (4), 1906657.
(142) Leng, J. S.; Lan, X.; Liu, Y. J.; Du, S. Y.; Huang, W. M.; Liu, N.; Phee, S. J.; Yuan, Q. Electrical Conductivity of Thermoresponsive Shape-Memory Polymer with Embedded Micron Sized Ni Powder Chains. *Appl. Phys. Lett.* **2008**, *92* (1), 014104.
(143) Mishra, S. R.; Tracy, J. B. Sequential Actuation of Shape-Memory Polymers through Wavelength-Selective Photothermal Heating of Gold Nanospheres and Nanorods. *ACS Appl. Nano Mater.* **2018**, *1* (7), 3063−3067.
(144) Manikandan, M.; Hasan, N.; Wu, H.-F. Platinum Nanoparticles for the Photothermal Treatment of Neuro 2A Cancer Cells. *Biomaterials* **2013**, *34* (23), 5833−5842.
(145) Toncheva, A.; Khelifa, F.; Paint, Y.; Voué, M.; Lambert, P.; Dubois, P.; Raquez, J.-M. Fast IR-Actuated Shape-Memory Polymers Using in Situ Silver Nanoparticle-Grafted Cellulose Nanocrystals. *ACS Appl. Mater. Interfaces* **2018**, *10* (35), 29933−29942.
(146) Bai, Y.; Zhang, J.; Wen, D.; Yuan, B.; Gong, P.; Liu, J.; Chen, X. Fabrication of Remote Controllable Devices with Multistage Responsiveness Based on a NIR Light-Induced Shape Memory Ionomer Containing Various Bridge Ions. *J. Mater. Chem. A* **2019**, *7* (36), 20723−20732.
(147) Sahoo, N.; Jung, Y.; Yoo, H.; Cho, J. Influence of Carbon Nanotubes and Polypyrrole on the Thermal, Mechanical and Electroactive Shape-Memory Properties of Polyurethane Nanocomposites. *Compos. Sci. Technol.* **2007**, *67* (9), 1920−1929.
(148) Chen, J.; Sun, D.; Gu, T.; Qi, X.; Yang, J.; Lei, Y.; Wang, Y. Photo-Induced Shape Memory Blend Composites with Remote Selective Self-Healing Performance Enabled by Polypyrrole Nanoparticles. *Compos. Sci. Technol.* **2022**, *217*, 109123.

https://doi.org/10.1021/acsomega.2c05930
ACS Omega XXXX, XXX, XXX−XXX

(149) Cortes, P.; Terzak, J.; Kubas, G.; Phillips, D.; Baur, J. W. The Morphing Properties of a Vascular Shape Memory Composite. *Smart Mater. Struct.* **2014**, *23* (1), 015018.
(150) Du, H.; Song, Z.; Wang, J.; Liang, Z.; Shen, Y.; You, F. Microwave-Induced Shape-Memory Effect of Silicon Carbide/Poly-(Vinyl Alcohol) Composite. *Sensors and Actuators A: Physical* **2015**, *228*, 1−8.
(151) Hasan, S. M.; Thompson, R. S.; Emery, H.; Nathan, A. L.; Weems, A. C.; Zhou, F.; Monroe, M. B. B.; Maitland, D. J. Modification of Shape Memory Polymer Foams Using Tungsten, Aluminum Oxide, and Silicon Dioxide Nanoparticles. *RSC Adv.* **2016**, *6* (2), 918−927.
(152) An, Y.; Okuzaki, H. Novel Electro-Active Shape Memory Polymers for Soft Actuators. *Jpn. J. Appl. Phys.* **2020**, *59* (6), 061002.
(153) Wang, X.; Lan, J.; Wu, P.; Zhang, J. Liquid Metal Based Electrical Driven Shape Memory Polymers. *Polymer* **2021**, *212*, 123174.
(154) Garces, I. T.; Aslanzadeh, S.; Boluk, Y.; Ayranci, C. Cellulose Nanocrystals (CNC) Reinforced Shape Memory Polyurethane Ribbons for Future Biomedical Applications and Design. *Journal of Thermoplastic Composite Materials* **2020**, *33* (3), 377−392.
(155) Lin, C.; Lv, J.; Li, Y.; Zhang, F.; Li, J.; Liu, Y.; Liu, L.; Leng, J. 4D-Printed Biodegradable and Remotely Controllable Shape Memory Occlusion Devices. *Adv. Funct. Mater.* **2019**, *29* (51), 1906569.
(156) Zhao, W.; Zhang, F.; Leng, J.; Liu, Y. Personalized 4D Printing of Bioinspired Tracheal Scaffold Concept Based on Magnetic Stimulated Shape Memory Composites. *Compos. Sci. Technol.* **2019**, *184*, 107866.
(157) Zhang, F.; Wen, N.; Wang, L.; Bai, Y.; Leng, J. Design of 4D Printed Shape-Changing Tracheal Stent and Remote Controlling Actuation. *International Journal of Smart and Nano Materials* **2021**, *12* (4), 375−389.
(158) Zhao, W.; Huang, Z.; Liu, L.; Wang, W.; Leng, J.; Liu, Y. Porous Bone Tissue Scaffold Concept Based on Shape Memory PLA/Fe3O4. *Compos. Sci. Technol.* **2021**, *203*, 108563.
(159) Yamagishi, K.; Nojiri, A.; Iwase, E.; Hashimoto, M. Syringe-Injectable, Self-Expandable, and Ultraconformable Magnetic Ultrathin Films. *ACS Appl. Mater. Interfaces* **2019**, *11* (44), 41770−41779.
(160) Babaie, A.; Rezaei, M.; Razzaghi, D.; Roghani-Mamaqani, H. Synthesis of dual-stimuli-responsive Polyurethane Shape Memory Nanocomposites Incorporating isocyanate-functionalized Fe_3O_4 Nanoparticles. *J. Appl. Polym. Sci.* **2022**, *139* (33), e52790.
(161) Wei, H.; Zhang, Q.; Yao, Y.; Liu, L.; Liu, Y.; Leng, J. Direct-Write Fabrication of 4D Active Shape-Changing Structures Based on a Shape Memory Polymer and Its Nanocomposite. *ACS Appl. Mater. Interfaces* **2017**, *9* (1), 876−883.
(162) Pineda-Castillo, S. A.; Luo, J.; Lee, H.; Bohnstedt, B. N.; Liu, Y.; Lee, C.-H. Effects of Carbon Nanotube Infiltration on a Shape Memory Polymer-Based Device for Brain Aneurysm Therapeutics: Design and Characterization of a Joule-Heating Triggering Mechanism. *Adv. Eng. Mater.* **2021**, *23* (6), 2100322.
(163) Wang, J.; Luo, J.; Kunkel, R.; Saha, M.; Bohnstedt, B. N.; Lee, C.-H.; Liu, Y. Development of Shape Memory Polymer Nano-composite Foam for Treatment of Intracranial Aneurysms. *Mater. Lett.* **2019**, *250*, 38−41.
(164) Paik, I. H.; Goo, N. S.; Jung, Y. C.; Cho, J. W. Development and Application of Conducting Shape Memory Polyurethane Actuators. *Smart Mater. Struct.* **2006**, *15* (5), 1476−1482.
(165) Kim, N.-G.; Han, M.-W.; Iakovleva, A.; Park, H.-B.; Chu, W.-S.; Ahn, S.-H. Hybrid Composite Actuator with Shape Retention Capability for Morphing Flap of Unmanned Aerial Vehicle (UAV). *Compos. Struct.* **2020**, *243*, 112227.
(166) Yang, S.; He, Y.; Liu, Y.; Leng, J. Non-Contact Magnetic Actuated Shape-Programmable Poly(Aryl Ether Ketone)s and Their Structural Variation during the Deformation Process. *Smart Mater. Struct.* **2022**, *31* (3), 035035.
(167) Cohn, D.; Zarek, M.; Elyashiv, A.; Sbitan, M. A.; Sharma, V.; Ramanujan, R. V. Remotely Triggered Morphing Behavior of Additively Manufactured Thermoset Polymer-Magnetic Nanoparticle Composite Structures. *Smart Mater. Struct.* **2021**, *30* (4), 045022.
(168) Peng, Q.; Wei, H.; Qin, Y.; Lin, Z.; Zhao, X.; Xu, F.; Leng, J.; He, X.; Cao, A.; Li, Y. Shape-Memory Polymer Nanocomposites with a 3D Conductive Network for Bidirectional Actuation and Locomotion Application. *Nanoscale* **2016**, *8* (42), 18042−18049.
(169) Xu, Z.; Wei, D.-W.; Bao, R.-Y.; Wang, Y.; Ke, K.; Yang, M.-B.; Yang, W. Self-Sensing Actuators Based on a Stiffness Variable Reversible Shape Memory Polymer Enabled by a Phase Change Material. *ACS Appl. Mater. Interfaces* **2022**, *14* (19), 22521−22530.
(170) Xu, L.; Li, Z.; Lu, H.; Qi, X.; Dong, Y.; Dai, H.; Islam Md, Z.; Fu, Y.; Ni, Q. Electrothermally-Driven Elongating-Contracting Film Actuators Based on Two-Way Shape Memory Carbon Nanotube/Ethylene-Vinyl Acetate Composites. *Adv. Materials Technologies* **2022**, *7* (7), 2101229.
(171) Hu, T.; Xuan, S.; Gao, Y.; Shu, Q.; Xu, Z.; Sun, S.; Li, J.; Gong, X. Smart Refreshable Braille Display Device Based on Magneto-Resistive Composite with Triple Shape Memory. *Adv. Materials Technologies* **2022**, *7* (1), 2100777.
(172) Dong, X.; Zhang, F.; Wang, L.; Liu, Y.; Leng, J. 4D Printing of Electroactive Shape-Changing Composite Structures and Their Programmable Behaviors. *Composites, Part A* **2022**, *157*, 106925.
(173) Ren, D.; Chen, Y.; Li, H.; Rehman, H. U.; Cai, Y.; Liu, H. High-Efficiency Dual-Responsive Shape Memory Assisted Self-Healing of Carbon Nanotubes Enhanced Polycaprolactone/Thermoplastic Polyurethane Composites. *Colloids Surf., A* **2019**, *580*, 123731.
(174) Orellana, J.; Moreno-Villoslada, I.; Bose, R. K.; Picchioni, F.; Flores, M. E.; Araya-Hermosilla, R. Self-Healing Polymer Nanocomposite Materials by Joule Effect. *Polymers* **2021**, *13* (4), 649.
(175) Cerdan, K.; Moya, C.; Van Puyvelde, P.; Bruylants, G.; Brancart, J. Magnetic Self-Healing Composites: Synthesis and Applications. *Molecules* **2022**, *27* (12), 3796.
(176) Melly, S. K.; Liu, L.; Liu, Y.; Leng, J. Active Composites Based on Shape Memory Polymers: Overview, Fabrication Methods, Applications, and Future Prospects. *J. Mater. Sci.* **2020**, *55* (25), 10975−11051.
(177) Chakraborty, D. D.; Chakraborty, P. Shape-Memory Polymer Composites and Their Applications. In *Smart Polymer Nanocomposites*; Elsevier: 2021; pp 103−115. DOI: 10.1016/B978-0-12-819961-9.00016-5.
(178) Cai, Y.; Jiang, J.-S.; Liu, Z.-W.; Zeng, Y.; Zhang, W.-G. Magnetically-Sensitive Shape Memory Polyurethane Composites Crosslinked with Multi-Walled Carbon Nanotubes. *Composites, Part A* **2013**, *53*, 16−23.
(179) Chen, S.; Yang, S.; Li, Z.; Xu, S.; Yuan, H.; Chen, S.; Ge, Z. Electroactive Two-Way Shape Memory Polymer Laminates. *Polym. Compos.* **2015**, *36* (3), 439−444.
(180) Cho, J. W.; Kim, J. W.; Jung, Y. C.; Goo, N. S. Electroactive Shape-Memory Polyurethane Composites Incorporating Carbon Nanotubes. *Macromol. Rapid Commun.* **2005**, *26* (5), 412−416.
(181) D'Elia, E.; Ahmed, H. S.; Feilden, E.; Saiz, E. Electrically-Responsive Graphene-Based Shape-Memory Composites. *Applied Materials Today* **2019**, *15*, 185−191.
(182) Dong, K.; Panahi-Sarmad, M.; Cui, Z.; Huang, X.; Xiao, X. Electro-Induced Shape Memory Effect of 4D Printed Auxetic Composite Using PLA/TPU/CNT Filament Embedded Synergistically with Continuous Carbon Fiber: A Theoretical & Experimental Analysis. *Composites, Part B* **2021**, *220*, 108994.
(183) Du, F.-P.; Ye, E.-Z.; Yang, W.; Shen, T.-H.; Tang, C.-Y.; Xie, X.-L.; Zhou, X.-P.; Law, W.-C. Electroactive Shape Memory Polymer Based on Optimized Multi-Walled Carbon Nanotubes/Polyvinyl Alcohol Nanocomposites. *Composites, Part B* **2015**, *68*, 170−175.
(184) Gong, T.; Li, W.; Chen, H.; Wang, L.; Shao, S.; Zhou, S. Remotely Actuated Shape Memory Effect of Electrospun Composite Nanofibers. *Acta Biomaterialia* **2012**, *8* (3), 1248−1259.
(185) Gu, S.-Y.; Jin, S.-P.; Gao, X.-F.; Mu, J. Polylactide-Based Polyurethane Shape Memory Nanocomposites (Fe_3O_4/PLAUs) with Fast Magnetic Responsiveness. *Smart Mater. Struct.* **2016**, *25* (5), 055036.
(186) Huang, C.-L.; He, M.-J.; Huo, M.; Du, L.; Zhan, C.; Fan, C.-J.; Yang, K.-K.; Chin, I.-J.; Wang, Y.-Z. A Facile Method to Produce PBS-

https://doi.org/10.1021/acsomega.2c05930
ACS Omega XXXX, XXX, XXX−XXX

PEG/CNTs Nanocomposites with Controllable Electro-Induced Shape Memory Effect. *Polym. Chem.* **2013**, *4* (14), 3987.
(187) Jimenez, G. A.; Jana, S. C. Composites of Carbon Nanofibers and Thermoplastic Polyurethanes with Shape-Memory Properties Prepared by Chaotic Mixing. *Polym. Eng. Sci.* **2009**, *49* (10), 2020−2030.
(188) Lee, S.-H.; Jung, J.-H.; Oh, I.-K. 3D Networked Graphene-Ferromagnetic Hybrids for Fast Shape Memory Polymers with Enhanced Mechanical Stiffness and Thermal Conductivity. *Small* **2014**, *10* (19), 3880−3886.
(189) Leng, J. S.; Huang, W. M.; Lan, X.; Liu, Y. J.; Du, S. Y. Significantly Reducing Electrical Resistivity by Forming Conductive Ni Chains in a Polyurethane Shape-Memory Polymer/Carbon-Black Composite. *Appl. Phys. Lett.* **2008**, *92* (20), 204101.
(190) Liu, X.; Li, H.; Zeng, Q.; Zhang, Y.; Kang, H.; Duan, H.; Guo, Y.; Liu, H. Electro-Active Shape Memory Composites Enhanced by Flexible Carbon Nanotube/Graphene Aerogels. *J. Mater. Chem. A* **2015**, *3* (21), 11641−11649.
(191) Lotfi Mayan Sofla, R.; Rezaei, M.; Babaie, A.; Nasiri, M. Preparation of Electroactive Shape Memory Polyurethane/Graphene Nanocomposites and Investigation of Relationship between Rheology, Morphology and Electrical Properties. *Composites, Part B* **2019**, *175*, 107090.
(192) Lu, H.; Liang, F.; Gou, J.; Leng, J.; Du, S. Synergistic Effect of Ag Nanoparticle-Decorated Graphene Oxide and Carbon Fiber on Electrical Actuation of Polymeric Shape Memory Nanocomposites. *Smart Mater. Struct.* **2014**, *23* (8), 085034.
(193) Luo, X.; Mather, P. T. Conductive Shape Memory Nanocomposites for High Speed Electrical Actuation. *Soft Matter* **2010**, *6* (10), 2146.
(194) Mahapatra, S. S.; Yadav, S. K.; Yoo, H. J.; Ramasamy, M. S.; Cho, J. W. Tailored and Strong Electro-Responsive Shape Memory Actuation in Carbon Nanotube-Reinforced Hyperbranched Polyurethane Composites. *Sens. Actuators, B* **2014**, *193*, 384−390.
(195) Orozco, F.; Kaveh, M.; Santosa, D. S.; Lima, G. M. R.; Gomes, D. R.; Pei, Y.; Araya-Hermosilla, R.; Moreno-Villoslada, I.; Picchioni, F.; Bose, R. K. Electroactive Self-Healing Shape Memory Polymer Composites Based on Diels−Alder Chemistry. *ACS Appl. Polym. Mater.* **2021**, *3* (12), 6147−6156.
(196) Park, J.; Dao, T.; Lee, H.; Jeong, H.; Kim, B. Properties of Graphene/Shape Memory Thermoplastic Polyurethane Composites Actuating by Various Methods. *Materials* **2014**, *7* (3), 1520−1538.
(197) Qi, X.; Dong, P.; Liu, Z.; Liu, T.; Fu, Q. Selective Localization of Multi-Walled Carbon Nanotubes in Bi-Component Biodegradable Polyester Blend for Rapid Electroactive Shape Memory Performance. *Compos. Sci. Technol.* **2016**, *125*, 38−46.
(198) Qi, X.; Xiu, H.; Wei, Y.; Zhou, Y.; Guo, Y.; Huang, R.; Bai, H.; Fu, Q. Enhanced Shape Memory Property of Polylactide/Thermoplastic Poly(Ether)Urethane Composites via Carbon Black Self-Networking Induced Co-Continuous Structure. *Compos. Sci. Technol.* **2017**, *139*, 8−16.
(199) Qian, C.; Zhu, Y.; Dong, Y.; Fu, Y. Vapor-Grown Carbon Nanofiber/Poly(Ethylene-Co-Vinyl Acetate) Composites with Electrical-Active Two-Way Shape Memory Behavior. *J. Intell. Mater. Syst. Struct.* **2017**, *28* (19), 2749−2756.
(200) Raja, M.; Ryu, S. H.; Shanmugharaj, A. M. Thermal, Mechanical and Electroactive Shape Memory Properties of Polyurethane (PU)/Poly (Lactic Acid) (PLA)/CNT Nanocomposites. *Eur. Polym. J.* **2013**, *49* (11), 3492−3500.
(201) Razzaq, M. Y.; Anhalt, M.; Frormann, L.; Weidenfeller, B. Thermal, Electrical and Magnetic Studies of Magnetite Filled Polyurethane Shape Memory Polymers. *Materials Science and Engineering: A* **2007**, *444* (1−2), 227−235.
(202) Razzaq, M. Y.; Behl, M.; Lendlein, A. Magnetic Memory Effect of Nanocomposites. *Adv. Funct. Mater.* **2012**, *22* (1), 184−191.
(203) Razzaq, M. Y.; Behl, M.; Nöchel, U.; Lendlein, A. Magnetically Controlled Shape-Memory Effects of Hybrid Nanocomposites from Oligo(ω-Pentadecalactone) and Covalently Integrated Magnetite Nanoparticles. *Polymer* **2014**, *55* (23), 5953−5960.
(204) Rogers, N.; Khan, F. Characterization of Deformation Induced Changes to Conductivity in an Electrically Triggered Shape Memory Polymer. *Polym. Test.* **2013**, *32* (1), 71−77.
(205) Sahoo, N. G.; Jung, Y. C.; Goo, N. S.; Cho, J. W. Conducting Shape Memory Polyurethane-Polypyrrole Composites for an Electroactive Actuator. *Macromol. Mater. Eng.* **2005**, *290* (11), 1049−1055.
(206) Schmidt, A. M. Electromagnetic Activation of Shape Memory Polymer Networks Containing Magnetic Nanoparticles. *Macromol. Rapid Commun.* **2006**, *27* (14), 1168−1172.
(207) Shao, L.; Dai, J.; Zhang, Z.; Yang, J.; Zhang, N.; Huang, T.; Wang, Y. Thermal and Electroactive Shape Memory Behaviors of Poly(l-Lactide)/Thermoplastic Polyurethane Blend Induced by Carbon Nanotubes. *RSC Adv.* **2015**, *5* (123), 101455−101465.
(208) Tang, Z.; Sun, D.; Yang, D.; Guo, B.; Zhang, L.; Jia, D. Vapor Grown Carbon Nanofiber Reinforced Bio-Based Polyester for Electroactive Shape Memory Performance. *Compos. Sci. Technol.* **2013**, *75*, 15−21.
(209) Valentini, L.; Cardinali, M.; Kenny, J. Hot Press Transferring of Graphene Nanoplatelets on Polyurethane Block Copolymers Film for Electroactive Shape Memory Devices. *J. Polym. Sci., Part B: Polym. Phys.* **2014**, *52* (16), 1100−1106.
(210) Wang, Z.; Zhao, J.; Chen, M.; Yang, M.; Tang, L.; Dang, Z.-M.; Chen, F.; Huang, M.; Dong, X. Dually Actuated Triple Shape Memory Polymers of Cross-Linked Polycyclooctene−Carbon Nanotube/Polyethylene Nanocomposites. *ACS Appl. Mater. Interfaces* **2014**, *6* (22), 20051−20059.
(211) Wang, Y.; Zhu, G.; Cui, X.; Liu, T.; Liu, Z.; Wang, K. Electroactive Shape Memory Effect of Radiation Cross-Linked SBS/LLDPE Composites Filled with Carbon Black. *Colloid Polym. Sci.* **2014**, *292* (9), 2311−2317.
(212) Wang, W.; Liu, Y.; Leng, J. Recent Developments in Shape Memory Polymer Nanocomposites: Actuation Methods and Mechanisms. *Coord. Chem. Rev.* **2016**, *320*−*321*, 38−52.
(213) Wang, Y.; Ma, T.; Tian, W.; Ye, J.; Wang, X.; Jiang, X. Electroactive Shape Memory Properties of Graphene/Epoxy-Cyanate Ester Nanocomposites. *PRT* **2018**, *47* (1), 72−78.
(214) Wei, K.; Zhu, G.; Tang, Y.; Li, X.; Liu, T. The Effects of Carbon Nanotubes on Electroactive Shape-Memory Behaviors of Hydro-Epoxy/Carbon Black Composite. *Smart Mater. Struct.* **2012**, *21* (8), 085016.
(215) Wei, Y.; Huang, R.; Dong, P.; Qi, X.-D.; Fu, Q. Preparation of Polylactide/Poly(Ether)Urethane Blends with Excellent Electro-Actuated Shape Memory via Incorporating Carbon Black and Carbon Nanotubes Hybrids Fillers. *Chin J. Polym. Sci.* **2018**, *36* (10), 1175−1186.
(216) Xia, S.; Li, X.; Wang, Y.; Pan, Y.; Zheng, Z.; Ding, X.; Peng, Y. A Remote-Activated Shape Memory Polymer Network Employing Vinyl-Capped Fe_3O_4 Nanoparticles as Netpoints for Durable Performance. *Smart Mater. Struct.* **2014**, *23* (8), 085005.
(217) Xiao, Y.; Zhou, S.; Wang, L.; Gong, T. Electro-Active Shape Memory Properties of Poly(ε-Caprolactone)/Functionalized Multi-walled Carbon Nanotube Nanocomposite. *ACS Appl. Mater. Interfaces* **2010**, *2* (12), 3506−3514.
(218) Yakacki, C. M.; Satarkar, N. S.; Gall, K.; Likos, R.; Hilt, J. Z. Shape-Memory Polymer Networks with Fe_3O_4 Nanoparticles for Remote Activation. *J. Appl. Polym. Sci.* **2009**, *112* (5), 3166−3176.
(219) Zhang, F. H.; Zhang, Z. C.; Luo, C. J.; Lin, I.-T.; Liu, Y.; Leng, J.; Smoukov, S. K. Remote, Fast Actuation of Programmable Multiple Shape Memory Composites by Magnetic Fields. *J. Mater. Chem. C* **2015**, *3* (43), 11290−11293.
(220) Zhang, Z.; Dou, J.; He, J.; Xiao, C.; Shen, L.; Yang, J.; Wang, Y.; Zhou, Z. Electrically/Infrared Actuated Shape Memory Composites Based on a Bio-Based Polyester Blend and Graphene Nanoplatelets and Their Excellent Self-Driven Ability. *J. Mater. Chem. C* **2017**, *5* (17), 4145−4158.
(221) Zhang, F.; Xia, Y.; Wang, L.; Liu, L.; Liu, Y.; Leng, J. Conductive Shape Memory Microfiber Membranes with Core−Shell Structures and Electroactive Performance. *ACS Appl. Mater. Interfaces* **2018**, *10* (41), 35526−35532.

https://doi.org/10.1021/acsomega.2c05930
ACS Omega XXXX, XXX, XXX−XXX

(222) Zhang, X.-J.; Yang, Q.-S.; Shang, J.-J.; Liu, X.; Leng, J. The Shape Memory Properties of Multi-Layer Graphene Reinforced Poly(L-Lactide-Co-ϵ-Caprolactone) by an Atomistic Investigation. *Smart Mater. Struct.* **2021**, *30* (5), 055005.
(223) Zhou, J.; Li, H.; Liu, W.; Dugnani, R.; Tian, R.; Xue, W.; Chen, Y.; Guo, Y.; Duan, H.; Liu, H. A Facile Method to Fabricate Polyurethane Based Graphene Foams/Epoxy/Carbon Nanotubes Composite for Electro-Active Shape Memory Application. *Composites, Part A* **2016**, *91*, 292−300.

https://doi.org/10.1021/acsomega.2c05930
ACS Omega XXXX, XXX, XXX−XXX